J. Indian Inst. Sci.
A Multidisciplinary Reviews Journal
ISSN: 0970-4140 Coden-JIISAD

REVIEW ARTICLE

A Review on the Applications of "Catalysis Under 2D-Cover" for Small Molecule Activation

Athira Jayasankar[1] *and Sooraj Kunnikuruvan*[1,2*]

Abstract | Development of catalysts for the sustainable and energy-efficient valorisation of small molecules has gained much attention in recent years. In this regard, a large number of catalysts have been developed, especially organometallic and heterogeneous catalysts. However, the poor stability, selectivity, sintering, and poisoning effects limit the application of these catalysts. 'Confined catalysis', in which catalytic processes take place within a unique chemical environment created by confinement within the catalytic system, has emerged as an effective strategy to enhance the activity, selectivity, and stability of catalysts for small molecule activation. This review explores various two-dimensional (2D) confined catalytic systems and their applications in the conversion of small molecules such as CO_2, N_2, NH_3, H_2O, and O_2 into value-added products. Specifically, it highlights recent computational studies, offering insight into the effect of structure and electronic structure of the catalytic systems, interaction between molecules, catalyst surface in confined spaces, etc., on small molecule activation.

Keywords: *Confined catalysis, Catalysis under cover, Small molecule activation, Density functional theory, 2D-materials*

1 Introduction

Small molecules like CO_2, NH_3, N_2, CH_4, CO, H_2, H_2O, and O_2 serve as essential feedstocks in various industrial, electrochemical, and environmental processes.[1–3] Despite being abundant reservoirs of chemical energy, their inert nature necessitates the development of catalysts that assist in overcoming significantly higher kinetic barriers for their activation.[4–7] Nanocatalysis, where nanoparticles drive chemical reactions, combines the advantages of conventional homogeneous and heterogeneous catalysis while minimizing their respective limitations, has long been utilized as active catalysts for small molecule activation.[8–13] The high surface-to-volume ratio, the distinct electronic properties compared to bulk materials, and the tunable size and morphology collectively enhance the selectivity and catalytic activity of nanocatalysts.[8] The Haber–Bosch process for the direct synthesis of ammonia from N_2 and H_2 is a classic example, where the nano-sized iron particles are used as the catalyst.[13] Other notable examples, such as CO oxidation on Au/metal oxide catalysts, direct H_2O_2 synthesis from H_2 and O_2, and methanol synthesis from CO and CO_2, have highlighted the significant impact of nanoscale effects on catalytic properties.[3]

Despite their advantages, the extensive applications of nanocatalysts are hindered by various factors. Many of the catalytically active nanocatalysts are based on precious metals such as Pt, Au, etc., and ligands or other supports are crucial for their stabilisation. The unsaturation of the surface atoms of the catalysts makes them highly reactive, and they undergo agglomeration or sintering, especially for reactions under harsh reaction conditions. Since the catalytic performance

[1] *Department of Chemistry, Indian Institute of Technology Madras, Chennai, Tamil Nadu 600036, India.*
[2] *Centre for Atomistic Modelling and Materials Design and Centre for Molecular Materials and Functions, Indian Institute of Technology Madras, Chennai, Tamil Nadu 600036, India.*
**soorajk@iitm.ac.in*

Springer IISc PRESS

of nanoparticles is strongly influenced by particle size and morphology, processes such as particle agglomeration significantly affect their catalytic activity. Moreover, the environmental impact, toxicity, catalyst poisoning by the strong adsorption of the intermediates on the surface of the catalyst, and scalability of these materials are also concerns.[11,12,14–16] In this regard, the isolation of active sites within confined regions, nano-confinement, is an effective strategy, not only for addressing the challenges like stability and catalyst poisoning in nanocatalysis, but also for significantly enhancing the catalytic activity of various reactions.[17]

Nanoconfinement, whether through encapsulation in nanoscale cavities, pores, or channels, or by restricting molecules on 2D surfaces, profoundly influences the transport of molecules and reaction dynamics in heterogeneous catalysis. This occurs by altering the fundamental chemical and physical properties of the molecules under confinement.[18,19] Single-molecule super-resolution microscopy and fluorescence imaging studies show that confining reactive centers within nanoscale spaces enables precise control over adsorption strength, mass transport, and activation energy, thereby optimizing reaction efficiency and yield.[18,20] Hence, the concept of 'confined catalysis' has been effectively used by various groups over the years to develop efficient catalytic systems for a range of applications, such as chemical synthesis, energy storage, etc.[18,21]

Chemical reactions in confined environments display characteristics that are markedly different from those observed in the bulk environment. Within a confined region, the selectivity and reactivity of the substrate(s) get enhanced because of the proximity of the substrate and the catalyst active center.[22] In confined spaces, the spatial/electronic interactions between the catalysts and the reactant molecules influence their adsorption energies as well as the dissociation energy barriers, which in turn affect the mechanism and kinetics of the reaction under consideration.[23–25] The encapsulated substrate adopts specific conformations to fit the cavity, limiting its movement and reaction pathways, often leading to a reduced activation entropy.[24] In addition, confined environments inhibit the sintering or clustering of active nanoparticles while blocking access to species that could poison the catalyst.[17,25] Structural engineering approaches such as defect engineering, doping, heterostructuring, etc., that can modulate the thermodynamics and kinetics of target reactions in conjunction with confinement effects were found to enhance catalytic activity.[17,26]

Nanoconfinement scaffolds can be classified based on the geometry of the confined space as 0D (zero-dimensional), 1D (one-dimensional), and 2D (two-dimensional) systems.[17] Highly porous materials, such as zeolites, are examples of materials with 0D confinement effects, which play a crucial role in their success as sorbents and catalysts.[27–29] Nanotube channels, including carbon nanotubes (CNTs) and titanium nanotubes (TNTs), are examples of 1D nanoconfinement systems, characterized by their well-defined hollow structures that effectively confine the substrates and modulate their reactivity. In these materials, the degree of confinement depends primarily on the diameter of the confined space.[30] Here, the interfaces formed between neighbouring 2D layers or between 2D overlayers and a solid surface create distinctive confined environments for chemical processes.[17,31]

'Catalysis under 2D-cover', where reactions take place at the interface between a solid surface and a one-atom-thick 2D layer, is one kind of confined catalysis. Examples of such 2D layers include graphene, graphdiyne, h-BN (hexagonal boron nitride), and g-C_3N_4 (graphitic carbon nitride).[31] The atomically thin cover was found to modify the adsorption properties of the substrate, often resulting in improved reaction kinetics.[32–34] Furthermore, such covers can act as a protective shield, preventing the direct adsorption of other molecular species that may deactivate the catalyst and thus stabilising the highly reactive metal surface from oxidation.[35]

The application of confined catalysis has shown remarkable promise in various fields, particularly in environmental catalysis, where research focuses on the treatment of various pollutants, including volatile organic compounds (VOCs), inorganic gases, and toxic gases.[25,36] Notably, there has been growing attention to the catalytic systems that form a 2D-cover, owing to their superior catalytic activity for small molecule activation, especially for the production of CO_2, NH_3, CH_4 etc. from CO, N_2, CO_2, respectively.[31,34,37–40] For example, CO adsorption on different metal surfaces can be modulated by incorporating 2D overlayers, which enhance CO oxidation.[39] In this review, we explore the recent progress in the application of 'catalysis under a 2D-cover', for small molecule activation with special attention to the computational studies that scrutinized the mechanism and kinetics of these reactions.

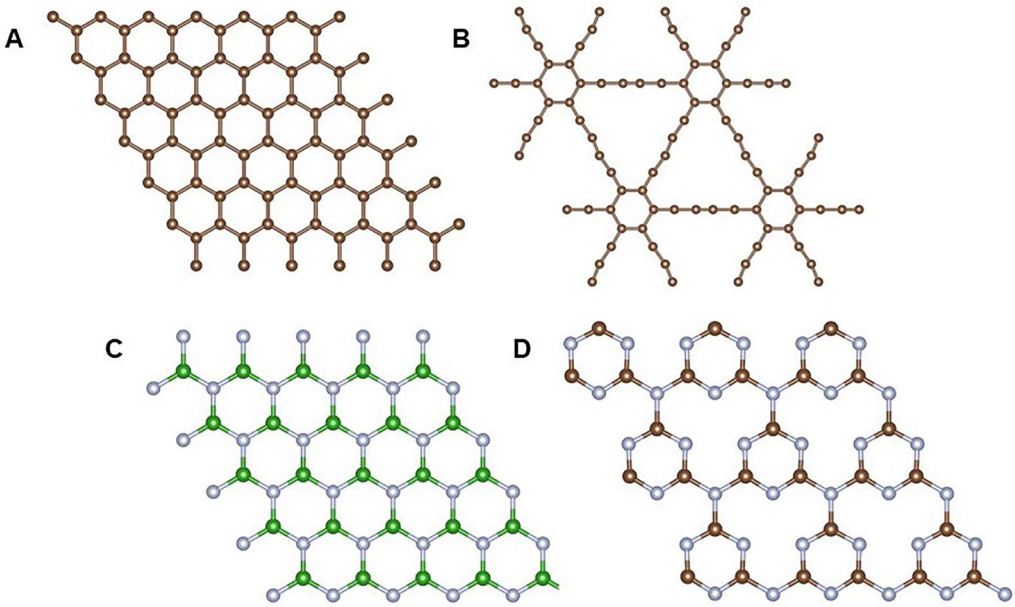

Figure 1: 2D-cover materials commonly used in confined catalysis. **A** graphene, **B** graphdiyne, **C** h-BN, and **D** g-C_3N_4.

2 Confinement Under 2D-Cover

'Catalysis under 2D-cover' is an emerging and promising approach to improve the catalytic activity of the materials by harnessing the unique characteristics of atomically thin 2-dimensional (2D) materials and confinement effects.[31,40] Catalytic systems employed in 'catalysis under 2D-cover' typically comprise 2D materials such as hexagonal boron nitride (h-BN), graphene, or graphitic carbon nitride (g-C_3N_4 supported on metal or metal oxide substrates. 2D materials can also be combined into heterostructures,[41,42] and the underlying components strongly influence the chemical properties of 2D materials.[42–44] Although the 'catalyst under 2D-cover' reaction can occur both thermally and electrochemically, we noted in passing that most of the reported studies are performed using electrochemical means. It is to be mentioned here that the controlled introduction of defects in 2D-covers during synthesis is crucial, since molecular intercalation generally follows a defect-assisted pathway. For instance, experimental studies on graphene-covered Pt(111) reveal that graphene islands with wrinkles are essential for the intercalation of small molecules such as CO at the interface.[45] Likewise, defects were found to have a significant role in CO intercalation between the Pt(111) surface and h-BN as well. For example, CO intercalation into h-BN nano-islands on Pt occurs at only 10^{-8} Torr, whereas a fully covered Pt surface prevents intercalation below 0.1 Torr CO.[46] However, in the presence of an applied potential, solvent molecules and solvated ions that are part of the electrolyte can infiltrate into the interfaces between 2D-covers and solid surfaces, enabling electrochemical reactions to occur beneath the 2D layer.

We noted that the majority of the experimental and computational studies reported over the years employed materials such as graphene, graphdiyne, h-BN, and g-C_3N_4 as the cover material. Notably, the potential of 2D materials such as MXenes, transition metal dichalcogenides (TMDCs), etc., as covers has not been explored yet. In the following sections, 2D materials (Fig. 1) that are widely used as covers for 'catalysis under 2D-cover' are discussed.

2.1 Graphene

Graphene, a 2D material with a honeycomb lattice and a monolayer of carbon atoms (Fig. 1A), is widely recognized for its characteristics, such as high thermal and electrical conductivity, mechanical strength, etc. Despite its impressive properties, pristine graphene typically exhibits poor catalytic activity due to its chemical inertness, and its activation has been explored using vacancies, impurity atoms, and substrate engineering.[47] Recent studies reveal that graphene as a cover on metal surfaces can enhance the catalytic properties of the latter for various reactions.[32]

The 2D confined space typically has a height of 3 Å, indicating that covered catalysis is limited to reactions involving small molecules. In such a catalytic system, the molecular and atomic species intercalate into the interfacial region within the graphene overlayer and the underlying metal or metal oxide surfaces, enabling catalytic reactions at the interface.[33,38] Experimental studies confirm that graphene is not only a protective layer but also actively influences underlying reactions in a controlled manner. Moreover, the orientation and adsorption energies of the molecules on the underlying catalyst surface were found to be modified in the confined space.[48] The weak adsorption of molecular species on the underlying metal can be ascribed to the electron transfer between carbon atoms in graphene and the adsorbate species.[33] As mentioned before, point defects and wrinkles in graphene can act as channels for molecular intercalation toward the interface. Moreover, the local chemical environment of graphene is altered by structural defects, including single and double vacancies.[49]

2.2 Graphdiyne

Graphdiyne (GDY) is a novel, sp/sp^2-hybridized carbon allotrope characterized by a one-atom-thick planar structure, where every hexagonal benzene ring is connected through 1,3-acetylenic linkages (Fig. 1B).[50–52] The presence of acetylenic linkages makes GDY more porous as compared to graphene. Computational studies by Jiao et al. showed that graphdiyne enables the permeation of H_2 molecules at a rate over 10^4 times faster than porous graphene even at room temperature.[53] For molecules such as N_2, CO, and CH_4, which have van der Waals sizes similar to the 5.4 Å pore size of GDY, the diffusion barriers are higher than those of H_2. Among these, CH_4 exhibits the highest diffusion barrier.[53,54] GDY-covered metal surfaces demonstrated enhanced catalytic performance in electrochemical reactions such as hydrogen evolution reaction (HER), oxygen reduction reaction (ORR), and CO_2RR than that of the bare metal surfaces.[38,55] Like graphene, the GDY cover stabilises the catalyst by forming a heterogeneous interface while weakening the adsorption of molecules that act as catalytic poisons on the metal surface.[55] Under electrochemical conditions, the agglomeration of metal nanoparticles is a major concern, as it diminishes their catalytic activity. For instance, Pt catalysts tend to lose activity during electrochemical reactions because of particle agglomeration, driven by their high surface energy. However, when covered with GDY, the interface formed between Pt and GDY prevents Pt particles from clustering and thereby enhances their stability and performance over multiple cycles.[55] Furthermore, the electronic structure of GDY significantly differs from that of graphene, exhibiting a quasi-particle band gap similar to that of silicon. Moreover, heteroatom doping in GDY, such as N, F, Cl, P, S, H, etc., offers an efficient method for modulating their properties, such as bandgap, conductivity, and charge distribution.[51] For example, nitrogen-doped graphdiyne (N/GDY) with more active sites, defects, and adsorption sites shows enhanced electrochemical properties than GDY.[56]

2.3 Hexagonal Boron Nitride

Hexagonal Boron Nitride (h-BN) is a layered inorganic material known for its thermal stability and high thermal conductivity (Fig. 1C). Progress in extracting atomically thin monolayers from layered crystals has significantly increased interest in mono- and few-layered h-BN, especially due to its potential as a wide-bandgap insulating material for diverse applications.[57,58] Although graphene and h-BN exhibit similar structures, they possess markedly different characteristics. In h-BN, the polarity arising from the partial ionic character of B–N bonds improves its affinity for small molecules relative to graphene.[59] In addition, h-BN is chemically and thermally stable in reactive environments, making it advantageous for chemical reactions.[60] Notably, atomically thin monolayers of h-BN can be grown on metal surfaces, where they have been proposed as highly selective and corrosion-resistant systems. The confined space formed in h-BN/metal systems serves as nano-reactors for catalytic applications, demonstrating the ability to facilitate molecule intercalation and confined catalysis, similar to the intercalation behaviour observed in graphene.[61,62] Various surface science techniques have proven the potential for molecular intercalation (such as O_2, H_2, CO, etc.) through h-BN layer.[31] The h-BN layer affects the adsorption characteristics of small molecules such as CO on the underlying metal surface, preventing CO poisoning by accelerating their desorption from the surface, even at room temperature.[46] These structural features enable the h-BN layer to serve as an effective facilitator as a cover for metal-catalyzed reactions.

2.4 Graphitic Carbon Nitride

Graphitic carbon nitride (g-C_3N_4) is known for its exceptional chemical and thermal stability

(Fig. 1D) and its planar structure closely resembles that of graphene and h-BN. The intrinsic porous structure of this material facilitates the intercalation of small molecules through triangular pores defined by six nitrogen atoms at their edges and enables their adsorption onto the underlying materials.[37,39] This makes g-C_3N_4 a good candidate as a cover in 'catalyst under cover'. Computational studies on g-C_3N_4-covered metal surfaces for electrochemical reactions indicate that the cover can modulate the binding energetics and scaling relation between the key intermediate species involved in the reaction. This is attributed to changes in the binding modes and binding energies of the intermediates on the metal surface under the cover, influenced by hydrogen bonding and steric confinement at the interface.[37,39]

3 Modeling Catalysis Under 2D-Cover

The role of 2D-covers in small molecule activation has been explored through computational studies, which provide detailed atomistic insights into interfacial interactions and reaction pathways. It also helps to capture the geometric and electronic effects imposed on these species under confinement. Some of the critical properties analyzed in these studies using computations include the adsorption of the molecule on the cover as well as the underlying metal surface, diffusion of molecules through the cover, mechanism of activation and value-added product formation from the small molecules, identification of critical reaction steps, and the electronic and structural factors that control the catalytic performance of the system under consideration. Density functional theory (DFT)-based computations in conjunction with the nudged elastic band (NEB) approach were widely used to study the mechanism, kinetics, and role of electronic and structural factors in determining the activity of various catalytic systems for small molecule activation.[63] NEB calculations are useful for determining the minimum energy pathway (MEP), offering insights into transport properties such as diffusion. In this case, it is particularly relevant to understand the diffusion of the molecule to and within the confined region. Details on the modeling of catalysts and some of the commonly used computational approaches are discussed in the following sub-sections.

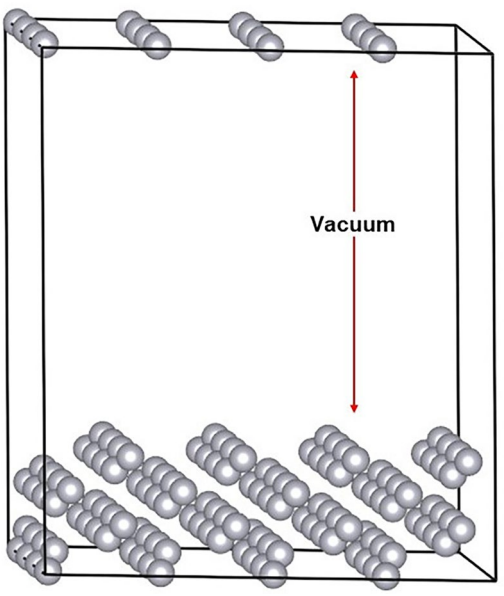

Figure 2: Surface-slab model with a vacuum layer in Z-direction.

3.1 Modeling of the Catalyst

In 'catalyst under 2D-cover', the catalysts have two main components:

(i) a one-atom-thick/single-layer 2D material that acts as the cover, and

(ii) the metal/metal oxide surface on which the reaction occurs. Here, the catalysts are modeled by placing a monolayer of the 2D material on top of metal/metal oxide surfaces, which are generated from their respective bulk along the desired direction, such that the lattice of the 2D material matches with that of the underlying material by minimizing the lattice mismatch. For instance, to model the metal surface covered by a monolayer of graphene, the lattice constant of the graphene overlayer needs to match that of a supercell of the underlying metal.[64] The lattice mismatch between the metal and the 2D-cover is calculated using the formula[65]:

$$\delta = (a_m - a_c)/a_m \quad (1)$$

where, a_m is the lattice constant of the metal, a_c is that of the 2D-cover, and δ represents the lattice mismatch between them.

Periodic-DFT calculations were extensively used to understand the structure, electronic structure, and their effect on the catalytic properties.[63,66,67] The surface properties of the materials are then studied using a surface-slab model where a vacuum layer is introduced on top of the cover to

avoid periodic interaction with the surface atoms of the image (Fig. 2).[63,68]. A vacuum thickness of about 12–16 Å was commonly employed in studies involving surface-slab models.[38,63,64,68,69]

3.2 Adsorption Energy and Free Energy Calculations

One of the key factors that determines the catalytic activity is the adsorption energy (E_{ads}) of the molecule (adsorbate) on the catalyst surface. E_{ads} can be estimated using the equation:

$$E_{ads} = E_{*\text{-adsorbate}} - E_{adsorbate} - E_{*} \quad (2)$$

where $E_{*\text{-adsorbate}}$ denotes the total energy of the system after the adsorption of the molecule, $E_{adsorbate}$ is the energy of the free adsorbate molecule/atom, and E_* denotes the total energy of the free catalyst. The feasibility of adsorption can be deduced from E_{ads}; a more negative E_{ads} suggests the preference for adsorption.[39]

DFT calculations in conjunction with phonon calculations are employed to compute the free energy, G, of the chemical species involved in the catalytic cycle using the formula below:

$$G = E + E_{ZPE} - TS \quad (3)$$

where T is the temperature, E is the total electronic energy of the system, E_{ZPE} is the zero-point energy and S represents the entropy.[64] The zero-point corrections and the entropy contributions can be computed using normal modes of vibration obtained from phonon calculations within the harmonic approximation. The free energy values thus obtained are then used to construct the free energy profile, which provides information on the effective free energy barriers and critical steps that control the catalytic activity. Some of the commonly used levels of theory for small molecule activation are provided in Table 1.

Table 1: Commonly used levels of theory for studying small molecule activation reactions.

System	Level of theory	vdW correction	Applications	Ref.
Gr/Ni(111)	PAW pseudo potentials and GGA of PBE	DFT-D2	HER	64
Gr/Pt(111)	PAW	PBE-D3	HER	70
Gr/Ni(111), Gr/Cu(111)	BLYP functional, DZVP basis set	Grimme's D3 method	HER	71
Gr/Pt(111), h-BN/Pt(111), g-C_3N_4/Pt(111)	PAW pseudo potentials and GGA of PBE	DFT-D3 with Becke–Johnson damping function	H_2O dissociation	72
Gr/Ni(111)	PAW using PBE potentials	rev-vdw-DF2 functional	HER	69
Gr/Pt(111)	PAW using PBE potentials	C^6/R^6 pair potentials (PBE-D)	CO oxidation	33
Gr/Pt(111)	PAW pseudo potentials and GGA of PBE	C^6/R^6 pair potentials (PBE-D)	ORR	32
Gr/Pt(111)	AIMD using PAW pseudo potentials and GGA of PBE	DFT-D2, DFT-D3, vdW-DF2	CO oxidation	73
Gr/M ; M = Ag, Au, Cu, Ni, Pd, Pt and Rh	PAW pseudopotentials with GGA	optB88-vdW	CO_2RR	74
Transition metal-doped Gr/Ni(111)	PAW pseudo potentials and GGA of PBE	DFT-D3	ORR	75
Porous Gr/NiO_x	PAW using PBE potentials	Grimme's DFT-D2 method	OER	76
GDY/Pt(111)	PAW using PBE potentials	Grimme's DFT-D2	CO oxidation	77
g-C_3N_4/Pt(111)	PAW pseudo potentials and GGA of PBE	vdW-DF method & optPBE-vdW functional	CO oxidation	39
g-C_3N_4/Ru(001)	PAW using PBE potentials	DFT-D3	eNRR	37
g-C_3N_4/Fe_{19}/BP	PAW approach	optPBE-vdW	eNRR	78
C_2N/Pt(111)	PAW pseudo potentials and GGA of PBE	DFT-D3	CO oxidation	34
N-C/Cu	PAW using PBE potentials	Grimme's DFT-D3	CO_2RR	79
h-BN	PAW using PBE potentials	Grimme's DFT-D2 method	CO intercalation	80

The following abbreviations are used in the column 'Applications': **HER** Hydrogen Evolution Reaction, ORR Oxygen Reduction Reaction, OER Oxygen Evolution Reaction, eNRR Electrochemical Nitrogen Reduction Reaction

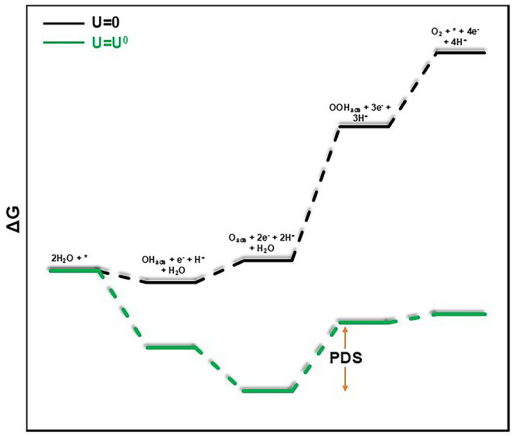

Figure 3: Schematic representation of free energy profiles for oxygen evolution reaction at $U = 0$ and $U = U^0$, the equilibrium potential. The PDS for the reaction is also shown.

3.3 Computational Hydrogen Electrode Model

DFT-based calculations can effectively determine the adsorption energetics of different species on metal surfaces. However, under a given potential, accurately calculating the energy of solvated protons and electrons in an electrocatalytic system is still challenging. The computational hydrogen electrode (CHE) model, established by Nørskov et al.[81] accounts for the chemical potential of proton-electron pairs without explicitly calculating their free energy. According to this model, the chemical potential for a proton-electron pair is equal to the chemical potential of gaseous hydrogen at 1 bar pressure and 298K under the potential of 0 V. That is, for a proton-electron pair, the equilibrium reaction is considered to be:

$$\mathrm{H}^+ + \mathrm{e}^- \rightarrow \frac{1}{2}\mathrm{H}_2(g)$$

at any pH and equilibrated at 0 V, and the corresponding free energy relation is given by,

$$G(H^+) + G(e^-) \rightarrow \frac{1}{2}G(H_2) - eU \qquad (4)$$

where U is the applied bias with respect to the reversible hydrogen electrode (RHE) and e is the elementary positive charge. Thus, the adsorption energy change for the reaction intermediates with n proton-electron pairs is given by,

$$\Delta G = \Delta E_{DFT} + \Delta ZPE - T\Delta S - neU \qquad (5)$$

where, ΔE_{DFT} is the binding energy calculated through DFT, ΔZPE is zero-point energy, $T\Delta S$ is the entropy correction at an applied potential U.[82]

Determining the potential-determining step (PDS) for different catalysts is a widely used method for identifying the most efficient catalyst and comparing the catalytic performance. For reactions involving multiple intermediates, DFT-based free energy calculations could suggest the PDS along the catalytic cycle if the free energy profile for the reaction is available.[83] Along the free energy profile computed at the equilibrium potential of the reaction, the step with the greatest free energy change is referred to as the PDS. A schematic free energy profile for OER, highlighting the associated PDS at the equilibrium potential (U^0), is shown in Fig. 3.

Overpotential, η $(U_{\text{applied}} - U^0)$ is another important parameter to evaluate their activity of electrocatalysts. More efficient catalysts exhibit a lower η value.[84] From the free energy profile, η can be estimated as the difference between the onset potential (U_{onset}) and the equilibrium potential, where,

$$U_{onset} = max((\Delta G_1, \Delta G_2, \Delta G_3, \ldots)/e)$$

Here, ΔG_i is the corresponding free energy difference between the elementary steps involved, and e is the charge of an electron.[85,86]

3.4 Diffusion Studies

Diffusivity of the adsorbates through the cover is a critical parameter that affects the efficiency of confined catalytic systems. In this regard, it is critical to understand the potential diffusion pathways and the corresponding diffusion barriers. One of the widely used approaches to identify the minimum energy path (MEP) for the diffusion and the barrier associated with it is the nudged elastic band (NEB) method.[87–89]

In NEB, a minimum energy path connecting two predefined minima (corresponding to the reactant and product) on the potential energy surface (PES) will be identified iteratively. Here, the path is composed of potential configurations connecting the reactant and the product, and these intermediate configurations can be generated using linear interpolation schemes. The intermediate configurations or images along the path between the two fixed minima along the PES are connected by harmonic springs to form an elastic band, where each configuration acts as a node along the band (Fig. 4).

Since none of the images are in their equilibrium configuration, a force equivalent to the

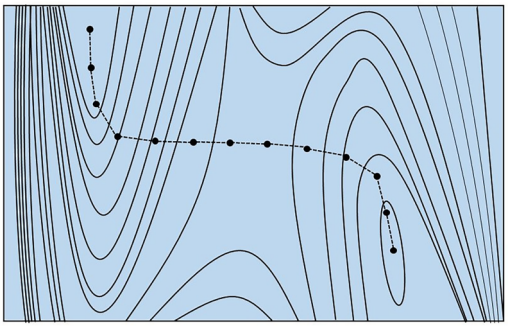

Figure 4: A schematic representation of the path connecting the reactant and product in NEB calculations. The PES is shown as a contour plot. The black dots along the MEP (indicated by the curve) are the images or nodes used in NEB calculations.

negative gradient of potential will be acting on each of these images, and the configurations thus displace towards the lower energy regions/local minima on the PES to minimise these forces. Since such a movement of individual configuration is not expected to provide the MEP, it is crucial to keep the images evenly spaced along the band, which is achieved by using a spring force. Thus, identifying MEP is essentially related to minimizing the energy of the elastic band, and the images need to be displaced simultaneously based on the net force on the elastic band. Herein, the net force is composed of two components, a perpendicular component of the force on each image ($F_\perp$) which directs the path towards MEP and the spring force (F_s) which acts along the path and controls the image distribution along the path. Therefore, the net force on each image i is given by:

$$\mathbf{F}_i = \mathbf{f}^S_{i,\parallel} - \mathbf{f}_{i,\perp} \tag{6}$$

where, $\mathbf{f}_{i,\perp}$ can be obtained from the total force $\mathbf{f}_i$, which is the negative gradient of the potential, by subtracting the projection of the component of $\mathbf{f}_i$ along the unit tangent along the path at the image i as given below:

$$\mathbf{f}_{i,\perp} = \mathbf{f}_i - (\mathbf{f}_i.\hat{\tau}_i)\hat{\tau}_i \tag{7}$$

Here, $\mathbf{f}^S_{i,\parallel}$ which is tangential to the path is given by,

$$\mathbf{f}^s_{i,\parallel} = (k^s_i|\mathbf{R}_{i+1} - \mathbf{R}_i| - k^s_{i-1}|\mathbf{R}_i - \mathbf{R}_{i-1}|).\hat{\tau}_i, \tag{8}$$

where k^s_is are spring constants and R_i are the atomic coordinates of the image i. The NEB method thus provides the MEP by displacing the images according to Eq. (6), and the convergence of the search for MEP is analysed by comparing the force on each image against a threshold value. The same spring constant is commonly used for all springs to ensure an even image distribution in NEB calculations. However, varying the spring constants can produce a different image distribution.

To accurately determine the barrier for the transition from the reactant to the product, it is crucial to have one of the images at the highest energy point along the path, and this can be achieved by using the climbing image NEB (CI-NEB) method.[89] In CI-NEB, the highest-energy image is shifted to climb toward and converge on the saddle point along the reaction path by treating the force on this image differently from the other images. Here, the parallel component of the atomic force on the climbing image, which is omitted in NEB calculations, will be inverted and added to the NEB force, and this image is unaffected by the spring forces. An accurate estimation of the diffusion barrier will help to predict the diffusivity of the molecules through the covers in confined catalysts because diffusivity through the cover often follows the Arrhenius equation. More details on the NEB and CI-NEB method can be found elsewhere.[89–91]

In addition to NEB/CI-NEB, the diffusion studies can also be computed using MD and kinetic Monte-Carlo (kMC) simulations. Here, the Einstein equation, which relates the diffusion coefficient to the mean square displacement computed using MD or kMC, is commonly used. We noted in passing that despite their advantages, very few studies employed molecular dynamics (MD), especially *ab initio* MD (AIMD) simulations for studying confined catalysis.

4 Applications of Catalysis Under 2D-Cover

The applications of catalysis under 2D-covers span various small molecule activation processes, including the water splitting, oxygen reduction reaction (ORR), electrochemical nitrogen reduction reaction (eNRR), CO oxidation, and CO_2 reduction reaction (CO_2RR). This section explores how 2D-covers influence the adsorption, charge transfer, and reaction pathways for the aforementioned reactions on different confined catalytic systems and thereby enhance the catalytic activity.

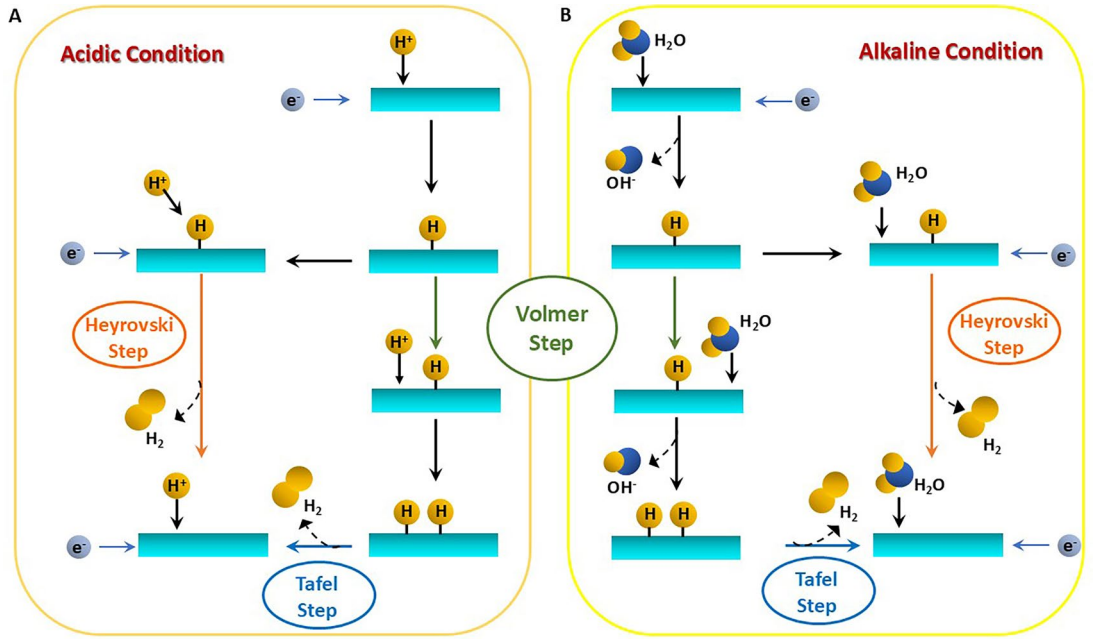

Figure 5: HER mechanism under **A** acidic conditions and **B** alkaline conditions. Adapted with permission from[96] Copyright 2018 © Springer Nature.

4.1 Hydrogen Evolution Reaction

Hydrogen evolution reaction (HER) is the reaction that occurs at the cathode in electrochemical water splitting and is one of the most extensively studied processes in electrocatalysis.[92] HER involves the adsorption of hydrogen at the electrode surface, with the reaction kinetics highly dependent on the adsorption energy, which varies according to the electrode material.[93] Platinum (Pt) is a widely used catalyst for HER due to its high electrochemical activity and stability in acidic environments. However, the limited availability and high cost of Pt limit their application as HER catalysts. To overcome this, the development of non-noble metal-based catalysts with low-cost, acidic stability, and HER activity comparable to Pt is crucial. Recent experimental and computational studies indicate that the presence of a 2D overlayer can significantly enhance the performance of non-precious metal catalysts and existing noble-metal catalysts for HER.

4.1.1 Mechanism of HER

HER is a multi-step electrochemical process that can take place in acidic, alkaline, or neutral media.[94,95] The schematic diagram of the mechanism for HER in acidic and alkaline environments is depicted in Fig. 5.[96–98]

The reaction begins with proton adsorption on the catalytic surface and is known as the Volmer step. The surface hydrogen then combines either with another proton from the solution (Heyrovsky step) or with another neighbouring surface hydrogen (Tafel step) to form a H_2 molecule. The chemical equations for these steps under alkaline/neutral conditions are given below:

Volmer:

$$M + H_2O + e^- \rightarrow M - H_{ads} + OH^-$$

Heyrovsky:

$$M - H_{ads} + H_2O + e^- \rightarrow M + H_2 + OH^-$$

Tafel:

$$M - H_{ads} + M - H_{ads} \rightarrow 2M + H_2$$

In acidic conditions, the Volmer and Heyrovsky step involves the protons and the Tafel step remains unchanged:

Volmer:

$$M + H^+ + e^- \rightarrow M - H_{ads}$$

Heyrovsky:

$$M - H_{ads} + H^+ + e^- \rightarrow H_2$$

Herein, the Heyrovsky and Volmer steps are preferred under low and high surface active site

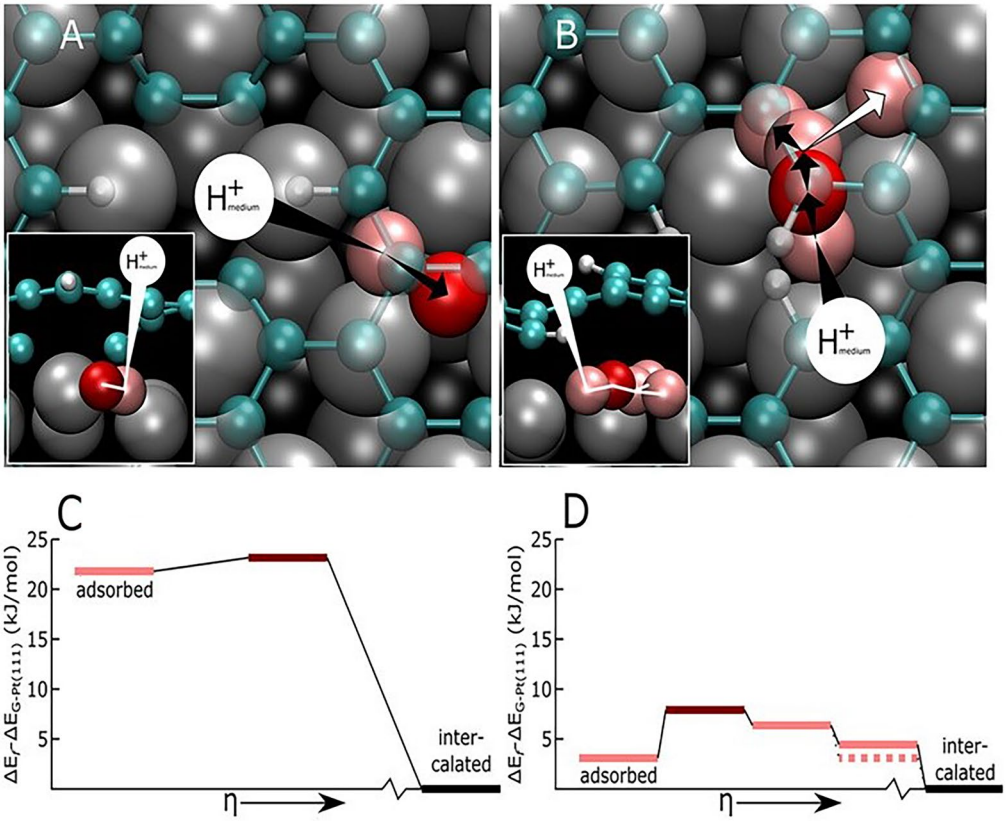

Figure 6: **A, B** Top view schematics of *H transport across far and close divacancies, respectively, by inset side views oriented along the plane of vacancy. The expected transport trajectories are marked with arrows. (cyan-C, white-H atoms bound to vacancy, grey/black-Pt, white circle-H^+ in the medium, red-*H at the barrier, pink-*H elsewhere). **C, D** Thermodynamic profiles of the minimum-energy permeation paths of *H through far and close divacancies, respectively. Reprinted with permission from[70] Copyright © 2023, American Chemical Society.

densities, respectively. 'M' represents the catalyst surface.

The $M-H_{ads}$ bond strength is one of the most critical factors in determining the HER activity of a catalyst and, for an ideal catalyst, the binding energy of 0 V which according to the Sabatier principle indicates a balance between H adsorption and H_2 desorption.[99,100] Thus, hydrogen binding energy is widely regarded as a key descriptor for HER activity in electrocatalysts.[101]

4.1.2 HER Under 2D-Cover

Platinum is a prominent catalyst for HER, owing to its superior electrochemical performance and remarkable chemical stability under highly acidic environments. Various experimental studies conducted for the selective permeation of ions through graphene in graphene (Gr)-covered Pt(111) systems (Gr/Pt(111)) indicate that protons selectively transport through graphene while inhibiting other bulky anions, cations, and water molecules towards the interface.[102,103] Combined experimental and theoretical studies by Kosmala et al. reported that in the confined inter-space within Gr and platinum (with optimal 3.7 Å gap), the HER is thermodynamically more favourable ($\Delta G_{H*} = -0.20$ eV) compared to the clean Pt(111) surface ($\Delta G_{H*} = -0.27$ eV).[103] The DFT calculation (GGA+D3 level of theory) by Arulmozhi et al. indicates that this lowering of H-adsorption energy in the interface can be attributed to the van der Waals interactions between pristine graphene and the Pt(111) surface.[70] However, this system is constrained by the limited diffusion of H_2 molecules away from the confined space.[103] Experimental studies by Shih et al. revealed that overlayers of graphene with defects on Pt(111) surfaces can surpass bare Pt(111) in catalytic performance for HER.[104] They showed that transport of H^+ and H_2 across the graphene overlayers occurs through the defects.

A decreased defect density in the graphene layer limits the transportation of H^+ and H_2 across it. This leads to a higher H_2 transport per defect site, which ultimately causes the delamination of the graphene layer.[104] Using DFT calculation (PBE+D3 level of theory), the same group has analyzed the H diffusion barriers across the graphene layer by free energy calculations.[70] The calculated energy barrier for the H atom diffusion through the intact graphene layer from vacuum onto Pt(111) was found to be 190 kJ mol^{-1}. However, this barrier reduced drastically to the range of 8–23 $kJmol^{-1}$ when divacancies were introduced to the graphene layer in aqueous media (Fig. 6A–D), which indicates the importance of defects in graphene cover.[70]

This supports the experimental findings that a graphene layer containing a high density of point defects assists proton permeation and enhances reaction rates.[70] HER studies by Yasuda et al. in the presence of graphene(Gr)/Au(111) also suggest that the defects in graphene are vital for the diffusion to the metal surface. The scanning tunneling microscopy (STM) studies by these authors indicate that, though the intrinsic defects in graphene allow diffusion of protons through them, they have a high permeation barrier for H_2.

The linear relationship between the HER overpotential and the proton-penetration current in graphene-covered non-noble metal catalysts (Cu and Ni) was observed by Hu and co-workers.[71] This experimental observation suggests that HER activity is primarily controlled by proton penetration through the graphene layers. The significantly higher overpotential required for the Gr/Cu system compared to the Gr/Ni system indicates that the reaction predominantly occurs at the metal-graphene interface rather than on the graphene itself because of graphene's lower catalytic activity compared to the underlying metal. The barrier calculations show that defects in the presence of pyridinic nitrogen dopant lower the energy barrier for proton penetration. In addition, these dopants and structural defects were found to be critical for the efficient ejection of H_2 bubbles formed at the interface without significantly damaging the graphene layer. Furthermore, free energy barriers associated with proton hopping through bilayer SV-3N (single vacancy with three N-dopants) graphene sheets were found to be 1.56 eV, which is lower than that of a defect-free monolayer graphene (3.16 eV). This also confirms that proton penetration across multiple graphene layers occurs through hopping between N-dopants.[71]

Tiwari et al. analysed the effect of cover in water dissociation by considering three confined systems-Gr/Pt(111), h-BN/Pt(111), and g-C_3N_4 /Pt(111) using DFT calculations (PBE+D3 level of theory).[72] This study shows that the strong binding of H_2O, H, and OH on the Pt(111) surface depends on the type of the cover and the graphene cover was found to have the strongest effect, as seen from the lowest activation barriers for O–H bond dissociation of H_2O calculated using the CI-NEB method. The electronic structure of the catalyst remained largely unchanged in the presence of different 2D overlayers, with or without the adsorbates. However, these overlayers alter the geometry of H_2O and OH compared to the bare Pt surface. These geometric changes affect the local electronic environment of the adsorbed species, as reflected in shifts in density of states (DOS) peaks ($\leq$1eV) for the respective species.[72]

Studies have also explored the confinement effects on HER while using non-noble metal catalysts. Zhou and co-workers explored HER performance on graphene-covered transition and noble metals using DFT-based calculations (PBE GGA + D2 level of theory), showing that hydrogen adsorption becomes less favourable on different metal surfaces when a graphene overlayer is introduced. This weakening in adsorption energy ranges from 0.12 to 0.23 eV for different metals, and the Ni surface showed the greatest difference.[64] The weakening of hydrogen adsorption in the graphene-covered metal interface was attributed to the energy penalty required to lift the graphene layer and create sufficient space for adsorbed hydrogen. Among the systems studied, Gr/Ni(111) was identified as the most effective non-precious metal catalyst for HER as indicated by the volcano plot (Fig. 7A), and its catalytic activity was found to be comparable to bare Pt. The authors also noted that diffusion of H-adatoms on the Ni surface in the presence of a graphene layer (0.20 eV) is only 0.05 eV greater than that of the bare Ni surface (0.15 eV). This is attributed to the fact that graphene shifts hydrogen slightly closer to the Ni surface by approximately 0.07 Å, leading to a marginally greater charge depletion around the adsorbed H, as illustrated in the charge density difference plot (Fig. 7B, C).

Graphdiyne (GDY), characterized by its uniform nanopores, as a monolayer on Pt(111), provides better access for the small molecules towards the active sites of the metal than the pristine graphene overlayer.[55] DFT calculations (PBE GGA level of theory) by these authors showed

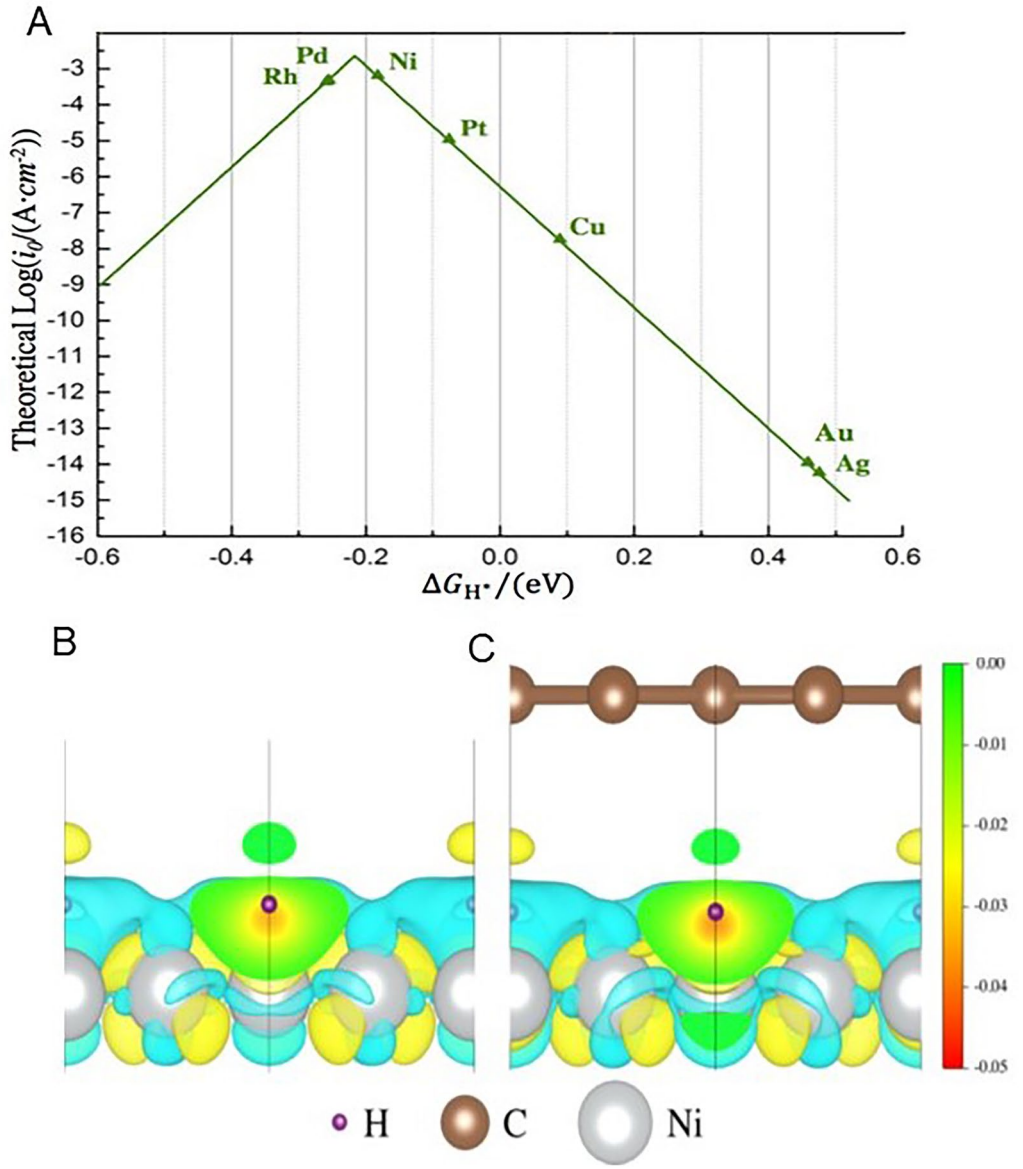

Figure 7: **A** Volcano curve showing the expected HER rates when the H adatom is confined within Gr/Metal interface. Charge density differences of **B** H on bare Ni and **C** H confined in Gr/Ni interface (Blue-charge depletion, yellow-charge accumulation, isovalue = 0.0025 e/$bohr^3$). Reprinted with permission from[64] Copyright © 2016, American Chemical Society.

that GDY monolayer on Pt(111) (GDY/Pt(111)) has a lower average overpotential (η) (0.26 V vs. RHE) as compared to bare Pt(111) (0.29 V vs. RHE), suggesting a superior HER activity for GDY/Pt(111) in contrast to bare Pt(111) surface. The authors also noted that the adsorption energies are dependent on the relative separation between GDY and Pt(111), indicating the 2D confinement effect.

4.2 Oxygen Evolution and Reduction Reactions

Oxygen evolution reaction (OER) is often identified as a key challenge in water electrolysis due to its inherently poor reaction rate, which reduces cell efficiency.[105,106] Metal oxides, perovskites, spinels, and carbon nanotubes (CNTs) are widely recognized catalysts for water electrolysis.[107] While metal oxide-based catalysts suffer from relatively low electrical conductivity, CNTs offer advantages such as high surface area, excellent conductivity, and strong corrosion resistance.[107]

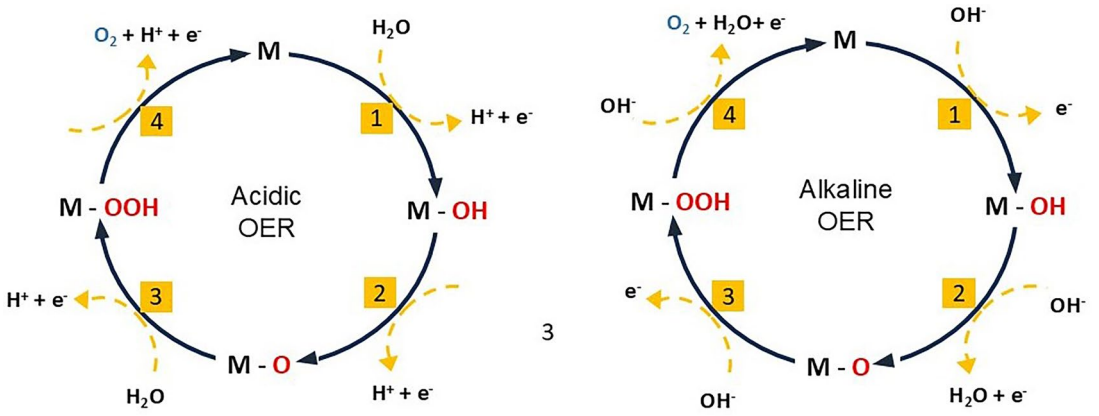

Figure 8: OER pathways under acidic and alkaline conditions. Reproduced from[115] with permission from the Royal Society of Chemistry.

Like OER, the oxygen reduction reaction (ORR) also exhibits sluggish kinetics due to challenges in O_2 adsorption on the electrode surface, O–O bond activation and cleavage, as well as oxide removal. Various Pt-based alloys (PtPd, PtAu, PtAg, PtCu, etc.) and core-shell structures (Cu@Pt, Ni@Pt, AuCu@Pt, etc.) have been reported for their catalytic efficiency for ORR.[108] To replace Pt, several cost-effective noble metal catalysts for ORR have been investigated, with Pd receiving significant attention due to its high activity and stability.[109,110] Introducing 2D confinement by covering the metal surface with a monolayer is a novel approach that has been found to enhance ORR activity and remains relatively unexplored.

4.2.1 Mechanism of OER

There are four electron/proton transfer steps in the widely accepted mechanism of OER.[111–113] DFT-based studies often focus on this four-step mechanism to evaluate the overpotential of the OER reaction on the catalyst surface under consideration for both acidic and alkaline conditions[97,98,111,112,114] (Fig. 8).

Under acidic conditions, the overall water oxidation reaction is given by the following equation:

$$2H_2O(l) \rightarrow O_2 + 4H^+ + 4e^- \quad \Delta E^0 = 1.23V_{RHE}$$

which follows the mechanism:

$$H_2O(l) + * \rightarrow *OH + H^+ + e^-,$$
$$*OH \rightarrow *O + H^+ + e^-,$$
$$H_2O(l) + *O \rightarrow *OOH + H^+ + e^-,$$
$$*OOH \rightarrow * + O_2(g) + H^+ + e^-,$$

and in alkaline media, the reaction proceeds through the following elementary steps:

$$OH^- + * \rightarrow *OH + e^-,$$
$$*OH + OH^- \rightarrow *O + H_2O(l) + e^-,$$
$$OH^- + *O \rightarrow *OOH + e^-,$$
$$*OOH + OH^- \rightarrow * + O_2(g) + H_2O(l) + e^-$$

Here, * represents the active site, (g) denotes the gas phase, and *OH, *O, and *OOH refer to the adsorbed species on the active site.

It has been demonstrated that, despite the apparent differences in individual reactions in acidic and alkaline conditions, the same equations can be applied to calculate key parameters like the overpotential and Gibbs free energy of reaction, provided the RHE is used as a universal reference. The CHE model (Sect. 3.3) is commonly employed for this in computational studies.[116]

4.2.2 Mechanism of ORR

The complex kinetics of ORR make its atomic-level mechanism challenging to understand fully. However, it is known that the electrochemical oxygen reduction comprises four proton-coupled electron transfers (PCETs) where the O_2 is being generated at the cathode.

The mechanism of ORR can vary depending on the catalyst, proceeding through either a four-electron mechanism, resulting in water formation, or a two-electron mechanism, forming hydrogen peroxide[117,118] (Fig. 9).

The overall reaction for the two-electron pathway leading to H_2O_2 is,

$$O_2 + 2(H^+ + e^-) \rightarrow H_2O_2 \quad E^0 = 0.70\ V$$

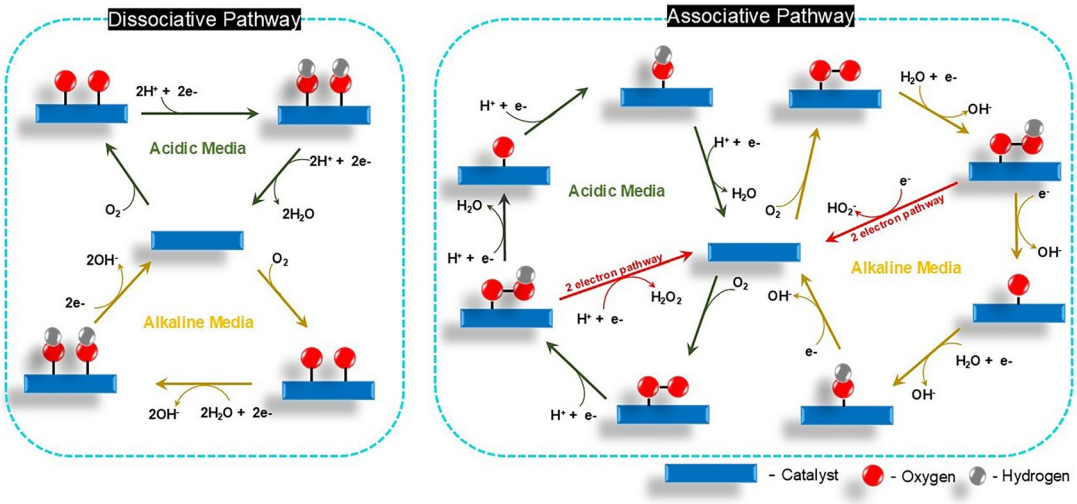

Figure 9: Schematic diagram of associative and dissociative mechanisms for ORR.

This partial reduction pathway proceeds via *OOH intermediate, and the elementary reaction involved can be written as:

$$O_2 + 2(H^+ + e^-) \rightarrow *OOH$$
$$+ (H^+ + e^-) \rightarrow H_2O_2$$

The four-electron pathway involves four sequential reduction steps, and based on the mode of adsorption of O_2, there are two pathways:

(i) Dissociative pathway: This route involves the bond breaking of O_2 followed by the hydrogenation of adsorbed oxygen (*O) to become *OH and H_2O . This mechanism (in acidic medium)is given by:

$$* + O_2 \rightarrow 2*O$$
$$2*O + 2(H^+ + e^-) \rightarrow 2*OH$$
$$2*OH + 2(H^+ + e^-) \rightarrow 2H_2O + *$$

(ii) Associative pathway: This pathway includes the formation of $*O_2$ (adsorbed molecular oxygen) followed by direct proton/electron transfer steps, proceeding through three key intermediates—*OOH, *O, and *OH .

$$* + O_2 \rightarrow *O_2$$
$$*O_2 + (H^+ + e^-) \rightarrow *OOH$$
$$*OOH + (H^+ + e^-) \rightarrow *O + H_2O$$
$$*O + (H^+ + e^-) \rightarrow *OH$$
$$*OH + (H^+ + e^-) \rightarrow H_2O + *$$

Thus, the overall reaction in the acidic medium is given as:

$$O_2 + 4(H^+ + e^-) \rightarrow 2H_2O \quad E^0 = 1.23\ V$$

Figure 9 represents these reaction pathways under both acidic and basic media.

4.2.3 OER and ORR Under 2D-Cover

The OER faces the challenge of requiring a substantial overpotential due to the inherently sluggish kinetics associated with the four-step proton-coupled electron transfer process.[119] First-row (3*d*) transition metal oxides (TMOs) have gained attention as effective non-noble metal-based electrocatalysts for OER, and different strategies have been explored to improve their performance.[120] However, the in situ surface reconstruction of these materials during OER forms a new oxide phase that often inhibits their catalytic activity and stability.[120] Xie et al. demonstrated improved photoelectrochemical (PEC) water oxidation using a Si-based photoanode covered with porous graphene (pGr) monolayer covering a NiO_x thin-film electrocatalyst.[76] Among the three photoanodes, n-Si/TiO_2/NiO_x, n-Si/TiO_2/NiO_x/Gr, and n-Si/TiO_2/NiO_x/pGr, compared, the pGr-covered photoanode exhibited the highest OER activity, as indicated by a photovoltage (Vph) of 382 mV. It shows that the improved PEC OER activity of the n-Si/TiO_2/NiO_x/pGr photoanode is mainly kinetically driven. PEC impedance spectroscopy further indicates that, unlike pristine graphene cover, there is an enhancement in the charge injection kinetics of the NiO_x electrocatalyst in the presence of pGr cover. The porous nature of pGr, with optimally sized pores, promotes oxygen and electrolyte diffusion across the layer. The authors showed that O_2 molecules generated during OER

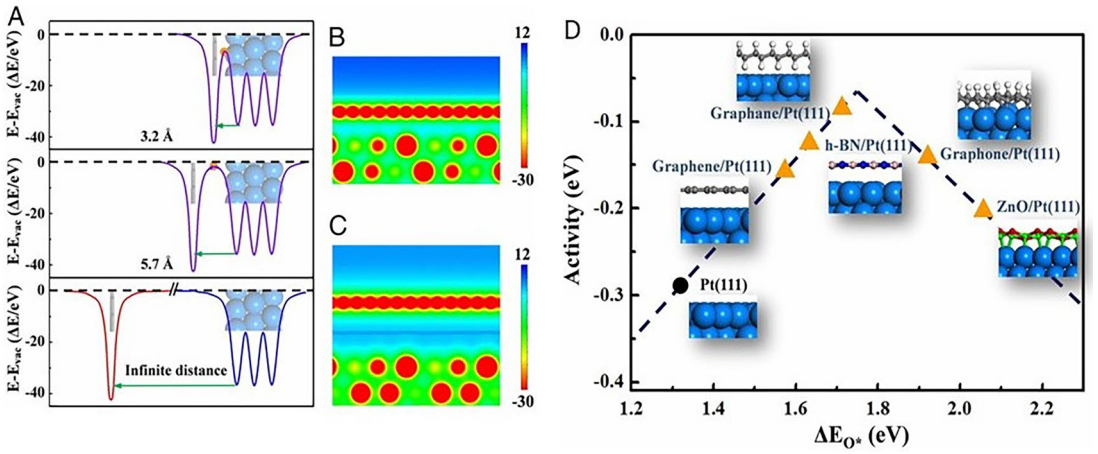

Figure 10: **A** One-dimensional local electrostatic potential distribution between Gr/Pt(111) surface at separations of 3.2 Å(top), 5.7 Å(middle), and an infinitely large distance (bottom), with the vacuum level defined as zero. Side-view of two-dimensional potential maps at the Gr/Pt(111) interface are shown for **B** 3.2 Å and **C** 5.7 Å separations. **D** The volcano plot of ORR activity as a function of ΔE_{O*} on Pt surface. Insets show representative interfacial atomic structures. Reprinted with permission from[32] Copyright ©, 2017, National Academy of Sciences, USA.

can pass through these pores without damaging the pGr layer, maintaining the structural stability of the catalyst. DFT-based (PBE-GGA level of theory)studies in this work indicate the formation of *OOH as the potential-limiting step. The authors also noted a higher overpotential for the pristine graphene-covered photoanode without pores (0.81 V). A comparison of the computed overpotentials between graphene covers with and without pores indicates a crucial role of the pores in lowering the overpotential. This is ascribed to the interaction between uncoordinated carbon atoms at defects and O* (and *OOH) species, which stabilises the reaction intermediates and thereby lowers the overpotential. Pt and its alloys consistently demonstrate superior catalytic activity for ORR.[121] Despite extensive research to develop cost-effective catalysts like graphene derivatives, TMOs, metal-organic frameworks, and dichalcogenides for ORR, their stability and electrocatalytic efficiency continue to pose challenges.[122–125] Ferrighi et al. demonstrated that the oxygen reactivity is significantly enhanced at the graphene/anatase TiO_2 interface, with a reduced energy cost for O_2 dissociation compared to the bare TiO_2 surface.[126] Rather than electronic effects, the formation of direct chemical bonds with the underlying substrate is primarily considered responsible for this enhancement. In addition, the authors also noted that boron doping in the graphene cover facilitates O_2 dissociation, making the process highly exothermic. Here, the boron atoms act as channels, transferring dissociated O atoms through the carbon layer into the interface. In contrast, nitrogen doping does not enhance the O_2 dissociation.[126]

Li et al. investigated the confinement effects on the surface reactivity of Pt-catalyzed ORR when various 2D layers such as monolayer graphene, h-BN, graphane, graphone, and g-ZnO are employed as covers.[32] The authors computed the binding energies of oxygen (ΔE_{O*}) on the catalyst surface (which is a commonly used descriptor for ORR), under various covers, using DFT-based studies (PBE+D2 level of theory). The volcano plot based on these calculations implies that graphene-based 2D-covers enhance the ORR activity, and graphane cover showed the most significant enhancement among them (Fig. 10D). The authors concluded that the geometric constraint and the 2D confinement are responsible for the weak adsorption of intercalated species on the metal surface by analyzing the electrostatic potential distribution in the confined environment. They showed that the Gr layer has a significant impact on the potential energy landscape close to the Pt(111) surface, as shown by the 1D potential distributions perpendicular to the Gr and Pt(111) surfaces at different Pt–Gr separation distances ($d_{Gr\text{-}Pt}$) (Fig. 10 A). The 2D potential distribution at these interfaces (Fig. 10B, C) reveals a distinct potential energy distribution in

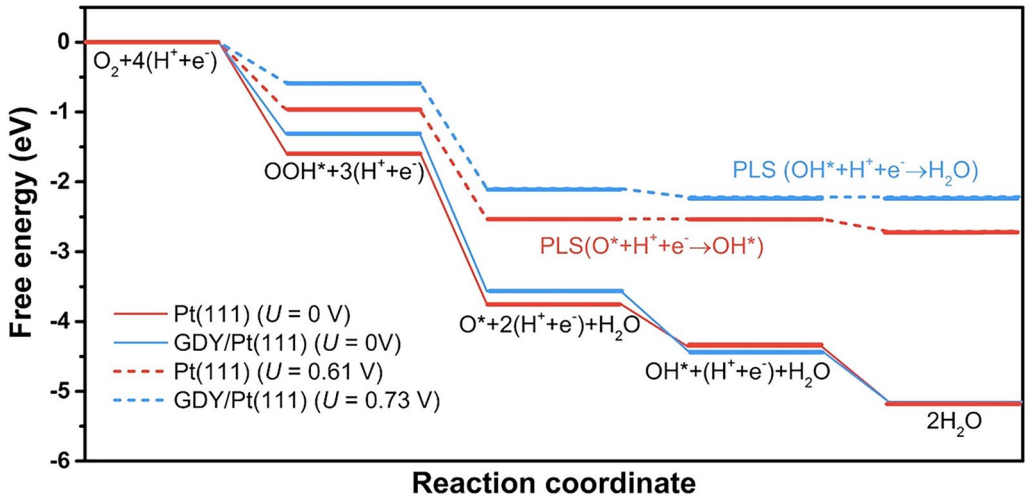

Figure 11: Free energy profiles for the ORR on Pt(111) surface and GDY/Pt(111) interface. Reprinted with permission from[55] Copyright © 2021, American Chemical Society.

the confined region beneath the Gr cover, which is absent in the case of the clean Pt(111) surface. This study indicates that adjusting the 2D microenvironment by modifying the cover can regulate surface reactivity, leading to improved ORR on the Pt metal.[32]

DFT-based calculations (PBE+D3 level of theory) by Chen et al. showed that the 2D confinement effect in the monolayer graphdiyne (GDY)/Pt(111) system disrupts the linear scaling relationship of adsorbed species (*OH, *O, and *OOH), leading to enhanced ORR activity.[55] By examining intermediate adsorption on the metal surface with and without a cover, they found that O adsorption is weaker (from 1.66 eV to 1.88 eV) under the influence of the GDY cover. However, the adsorption energies of OH and OOH remained nearly unchanged in both cases (Fig. 11). Charge density difference analysis showed that strong electrostatic attraction causes a stronger interaction among OH (OOH) and GDY at the interface, counterbalancing the weak adsorption caused by 2D confinement effects.

Herein, the solvent effects were incorporated using the COSMO (conductor-like screening model) implicit model with a dielectric constant of 78.54. Notably, the presence of the GDY cover altered the potential-limiting step from $*O + H^+ + e^- \rightarrow *OH$ (without cover) to $*OH + H^+ + e^- \rightarrow H_2O$ (with cover) as shown in Fig. 11. Furthermore, all active sites in the GDY/Pt(111) system exhibit lower overpotential (η) values for ORR (0.45–0.59 V) compared to bare Pt(111) (0.62 V), indicating superior catalytic performance.[55]

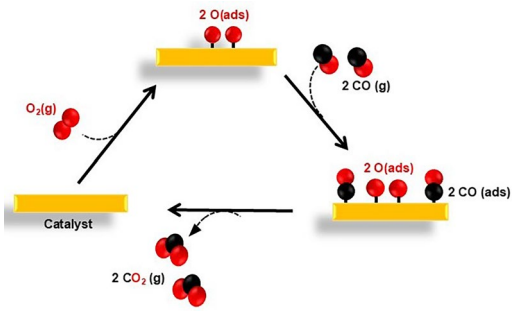

Figure 12: Langmuir–Hinshelwood scheme for CO oxidation reaction.

4.3 CO Oxidation

CO oxidation is an effective approach to reduce the rising CO emissions from coal combustion. CO oxidation proceeds via the adsorption of CO and O_2 on the catalytic surface, followed by the dissociation of O_2 and the subsequent reaction between adsorbed oxygen and CO molecules (Langmuir–Hinshelwood mechanism).[127] Catalysts for this reaction commonly include transition metals such as Au, Pt, and Pd.[128–130] However, CO oxidation faces challenges due to the low catalytic activity at lower temperatures, the instability of catalysts at higher temperatures, and the high cost associated with noble metal catalysts.[131] Moreover, strong CO adsorption on metal surfaces often outperforms O_2 adsorption, leading to catalyst poisoning, where CO occupies active sites, blocks O_2 dissociation, and inhibits the reaction.[132] Therefore, stable and cost-effective catalysts capable of fully converting CO to

products such as CO_2 without catalytic poisoning have gained significant attention.[131] Studies suggested that introducing a 2D layer on a metal surface can reduce catalytic poisoning by modifying the adsorption strength of CO.[32,45] Consequently, numerous experimental and computational investigations have explored the intercalation of CO under different 2D layers and their impact on metal surfaces under various reaction conditions.[73,133,134]

4.3.1 Mechanism of CO Oxidation

The widely accepted pathway for CO oxidation is the Langmuir–Hinshelwood (L–H) mechanism, which involves the following steps[135,136]:

$$* + O_2(g) \rightarrow 2^*O$$
$$* + 2CO(g) \rightarrow 2^*CO$$
$$2^*O + 2^*CO \rightarrow * + 2CO_2(g)$$

where, * represents the adsorbent, *CO and *O are the adsorbed species on the catalyst (Fig. 12). The overall CO oxidation reaction can be shown by the equation given below:

$$2CO + O_2 \rightarrow 2CO_2$$

The Eley–Rideal (E–R) mechanism is an alternative pathway for CO oxidation, where the reaction occurs between gaseous CO molecules and adsorbed oxygen atoms to generate gaseous CO_2 molecules. However, since CO is more likely to adsorb on the catalyst (L–H mechanism) rather than directly interact with adsorbed oxygen due to the higher energy barrier,[136] the L–H mechanism is generally preferred in most surface-catalyzed reactions, with only a few proceeding via the ER pathway.[137,138]

4.3.2 CO Oxidation Under 2D-Cover

Yao et al. investigated the Graphene/Pt(111) system to examine the impact of a 2D overlayer on the CO oxidation reaction by employing in situ surface science studies (PM-IRRAS, temperature-programmed desorption) and DFT-based computations (PAW-PBE+D level of theory).[33] This study reported a weaker interaction between CO and Pt under the influence of a graphene overlayer and thereby a lower reaction barrier for CO oxidation. CI-NEB-based assessment of reaction pathway showed that the TS configurations remained similar for both Pt(111) and Gr/Pt(111). However, the energy barrier on the bare Pt(111) surface is found to be 0.66 eV, which is lowered to 0.51 eV in the presence of graphene. Furthermore, charge density difference analysis of the TS atomic configuration reveals charge transfer from the Gr layer to the CO/O adsorbates, weakening the CO bond and facilitating O–CO bond formation. DFT calculations by Tiwari et al. further support the reduction in barrier in the presence of graphene, highlighting the strong van der Waals (vdW) interactions in Gr/metal systems by comparing results using functionals with and without vdW corrections. *Ab initio* molecular dynamics (AIMD) studies involving the post-transition state configurations for CO oxidation in the 2D confined region of the Gr/Pt(111) system by these authors reveal that there is a significant confinement effect at lower temperatures (90 K). Also, at this temperature, CO_2 desorbs sooner from the confined system than from the bare Pt(111) surface, and the geometry of the desorbing CO_2 was found to change when the graphene layer is introduced.[73] Li et al. further confirmed the attractive vdW interaction between Gr and Pt(111) through DFT-based studies and noted that Pt 'pushing' CO molecules toward the Gr layer. However, the Gr–CO interaction remains repulsive, suggesting that CO adsorption is weaker under confinement, which ultimately implies the geometric constraints imposed on the small molecules by the 2D microenvironment.

Zhang and coworkers explored the impact of 2D material covers on the catalytic surface behaviour of metal catalysts, focusing on the adsorption and oxidation of CO at the h-BN/Pt(111) interface through in situ surface techniques (LEEM, IRRAS and AP-XPS).[46] They found that the h-BN layer weakens CO adsorption on Pt, mitigating CO poisoning and enhancing CO oxidation at lower temperature conditions in contrast to the bare Pt(111) surface. Notably, a more pronounced effect of confinement is observed with h-BN covers relative to graphene layers, as complete CO desorption occurs near room temperature under h-BN, whereas graphene requires $\sim 100^\circ$ C for the same effect.[33] These observations were further supported by computations, where the authors noted a lower CO adsorption energy in the presence of graphene (1.57 eV) and h-BN (1.48 eV) covers as compared to bare Pt(111) (1.99 eV). The stronger confinement effect of h-BN is primarily attributed to its polar nature, in contrast to non-polar graphene. This results in strong electronic interactions with the metal surface, rather than being driven by geometric effects.[46] Additionally, both experimental and DFT calculations confirm the molecular enrichment effects on h-BN covered Pt surface.[80] In this study, Wu et al. showed

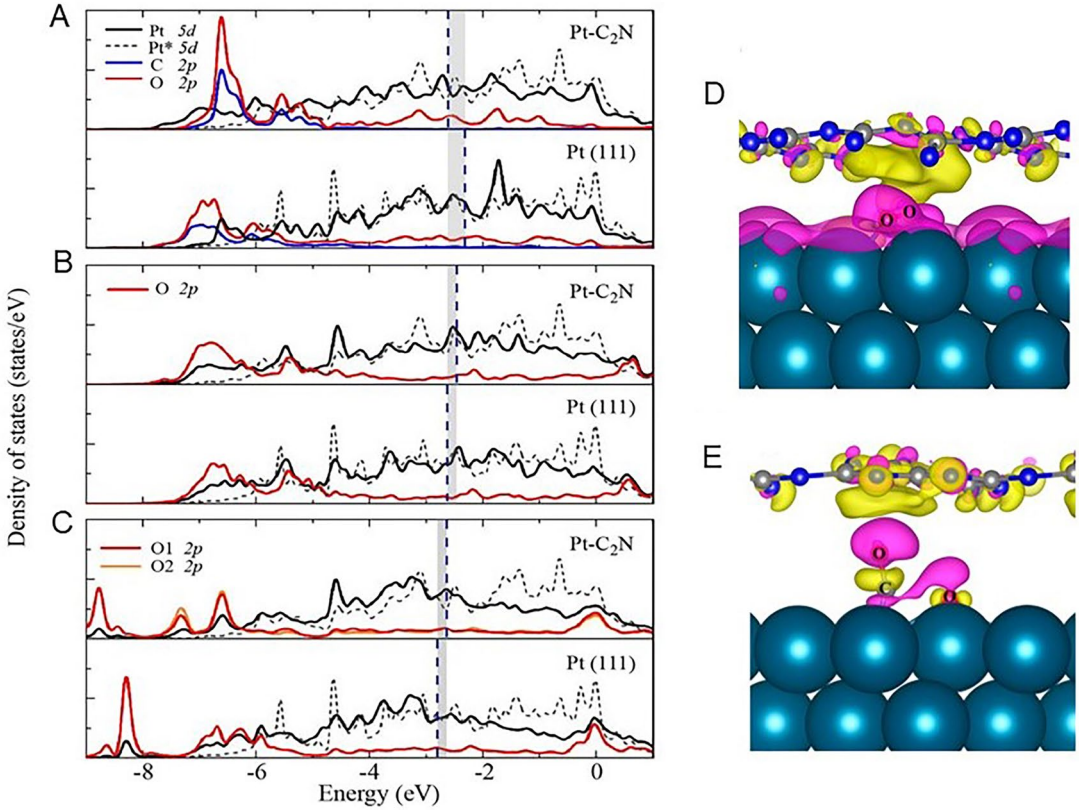

Figure 13: **A–C** PDOS plots for the Pt atom nearest to the adsorbed species—**A** CO, **B** O, and **C** O_2-shown both with and without C_2N coverage. (Dotted line curve—Pt atom without the adsorbate, solid line—Pt atom with the adsorbate, vertical dashed line—d-band center of activated Pt. Reprinted with permission from[34]; permission conveyed through Copyright Clearance Centre, Inc. The computed differential charge density of TSs for **D** O_2 dissociation and **E** CO oxidation at the interface of g-C_3N_4/Pt(111). (Yellow/Purple—charge depletion/accumulation, Atom color coding: C-gray, N-blue, O-red, Pt-indigo.) Reprinted with permission from[39] Copyright ©2017, American Chemical Society.

that under the same CO partial pressure, CO coverage on Pt(111) under h-BN is higher than that on a bare Pt(111) surface. A similar observation of more dispersed coverage of CO molecules was observed by Eads et al. in a 2D silica-covered Pd(111) system by employing in situ techniques (APXPS and IRRAS).[139] The formation of surface oxide from molecular oxygen, along with the dispersed coverage of CO, led to an improved CO_2 production under confinement. A 12% rise in CO_2 was reported as a consequence of the silica covering compared to the surface of clean Pd(111).[139] However, unlike the rapid CO adsorption observed on Pt(111) surfaces under h-BN islands upon CO exposure at room temperature, CO intercalation was absent under the defect-free h-BN layer.[46,48] This indicates the critical role of defects in the h-BN cover in facilitating reactions under the 2D layer, and the defect generation is often influenced by the synthesis conditions, resulting in their irregular formation.

Wang et al. has investigated CO oxidation on a Pt(111) surface covered with g-C_3N_4 employing DFT-based calculations (GGA-optPBE-vdW level of theory), leveraging its unique porous structure, which facilitates the intercalation of small molecules beneath the 2D layer. The interface formed in C_3N_4/Pt(111) system decreased the energy barrier associated with CO oxidation, indicating enhanced reactivity under confinement.[39] This improved catalytic performance is ascribed to charge transfer to the intercalated small molecules from the overlayer. Differential charge density analysis revealed substantial charge transfer from the C_3N_4 layer to the adsorbed CO and O_2 species (Fig. 13D, E). This accumulated charge causes the weakening of the O–O and C–O bonds, ultimately facilitating O–CO bond formation. In addition, the NEB calculations reported

in this work revealed that CO_2 and O_2 can permeate through the pores, and their binding on the metal surface can be modulated by the g-C_3N_4 cover.[39]

Guo and coworkers investigated the CO oxidation by employing Pt(111) surface-supported C_2N monolayer (belongs to h-BN family) as the catalyst with different configurations (top/fcc/hcp) using first-principles calculations (GGA-PBE+D3 level of theory).[34] Similar to other cases, the presence of the C_2N cover weakens CO adsorption (by 0.37 eV) compared to the bare surface of Pt(111). Although there is no significant electron transfer between C_2N and CO, a charge transfer between CO and Pt was observed. The authors reported that charge transfer from bare Pt(111) to CO is 0.17*e*, which decreases to 0.15*e* under the C_2N cover, indicating a weaker CO-Pt interaction in the confined space and, consequently, a weaker CO adsorption on the metal surface. This is further confirmed by observing a lowering of the d-band center of activated Pt in the absence (−2.32 eV) and presence (−2.62eV) of the C_2N cover (Fig. 13A). The authors also examined charge transfer between the Pt surface and adsorbed O atoms (and O_2) to gain further insight into the CO oxidation reaction. Charge analysis revealed that the presence of C_2N generates a weak electric field, stabilising the adsorbed O atom under the cover. Additionally, a d-band center shift towards the Fermi level was observed (Fig. 13B) for *O under C_2N cover confirms this stabilisation. Similar to the case of CO, the C_2N cover causes charge loss in the O–O bond, making O_2 much susceptible to dissociation and observed a slight d-band center shift towards the Fermi level (Fig. 13C). The preference of the C_2N /Pt (111) for the effective CO oxidation was further confirmed in this study by observing a positive adsorption energy for CO_2, the product molecule, under the effect of confinement.[34]

Eads et al. investigated CO oxidation on a Pd(111) surface in the presence and absence of a 2D silica cover using in situ techniques (APXPS and IRRAS).[139] They observed that the confined system demonstrated approximately 12% higher CO_2 production rates compared to the bare Pd surface. The 2D-cover promotes a more dispersed coverage of the adsorbed CO, which facilitate the reaction of O_2 on the surface, generating atomic oxygen and forming a surface oxide that subsequently reacts with CO to improve CO_2 production.[139]

4.4 CO_2 Reduction Reaction

CO_2 reduction reaction (CO_2RR) is a highly complex process comprising multi-electron/proton transfer, and a variety of different products ranging from small molecules such as CO, CH_4, etc. to higher hydrocarbons and alcohols.[140] The electrochemical reduction of CO_2 (eCO_2R) on different metal surfaces has been extensively investigated over the years.[141,142] For example, the conversion of CO_2 to CO has been reported to be enhanced on metals such as Au, Ag, Pd, Fe, etc., while Cu catalyses the production of hydrocarbons and alcohols from CO_2.[143] However, current catalysts require high overpotentials to achieve practical reaction rates and often exhibit poor selectivity for target products.[144–146] For instance, although Cu is the most effective metal electrocatalyst for CO_2RR, it exhibits a high onset voltage (~1 V) for CO_2 reduction to hydrocarbons.[144,147] Additionally, the competing HER is also a major reason for the low faradaic efficiency in CO_2 reduction (CO_2RR).[148,149] Other major challenges in CO_2RR include achieving selectivity for desired products while minimizing energy barriers, ambiguities in reaction pathways and mechanisms, and catalyst instability under operational conditions.[143]

To address these limitations, the application of 'confinement effects' in CO_2RR has shown several advantages, including enhanced initial CO_2 adsorption and activation, improved control over reaction pathways and selectivity via stabilization of key intermediates, and increased catalyst durability by protecting active sites from degradation.[143]

4.4.1 Mechanism of CO_2RR

In CO_2RR, the formation of intermediates is governed by the interaction of CO_2 with catalyst surfaces or electron-rich species. Some of the most commonly reported proton-coupled electron transfer reactions of CO_2 at pH 7 with reference to NHE, as documented in the literature, are given below[97,140]:

Carbon Monoxide

$$CO_2 + 2(H^+ + e^-) \rightarrow CO + H_2O \quad E^0 = -0.51\ V$$

Formaldehyde

$$CO_2 + 4(H^+ + e^-) \rightarrow HCHO + H_2O \quad E^0 = -0.55\ V$$

Methanol

$$CO_2 + 6(H^+ + e^-) \rightarrow CH_3OH + H_2O \quad E^0 = -0.39\ V$$

Methane

$$CO_2 + 8(H^+ + e^-) \rightarrow CH_4 + 2H_2O \quad E^0 = -0.24\ V$$

Acetaldehyde

$$2CO_2 + 10(H^+ + e^-) \rightarrow CH_3CHO + 3H_2O \quad E^0 = -0.36\ V$$

The fundamental steps of CO_2 reduction on transition metal surfaces are given by[74]:

$$CO_2 + H^+ + e^- \rightarrow *COOH$$
$$*COOH + H^+ + e^- \rightarrow *CO + H_2O$$
$$*CO + H^+ + e^- \rightarrow *CHO$$

The adsorption studies on pristine TM surfaces suggested that the scaling relation between the binding energies of the key intermediates involved in CO_2RR (E_b (COOH) and E_b (CO) as well as E_b (CHO) and E_b (CO)) limits the catalytic activity of these metals.[150,151] Therefore, enhancing CO_2 reduction activity requires decoupling the binding energetics of the intermediates on the transition metal surface. Peterson et al. suggested that the linear relationship between CO and CHO intermediates can be disrupted by alloying with metals that have higher oxygen affinity, introducing electrophilic chemical ligands, and stabilising intermediates through hydrogen bonding.[150]

4.4.2 CO_2RR Under 2D-Cover

The confined region between the metal surface and the overlying 2D material layer provides an optimal environment for enhancing the catalytic activity of CO_2 reduction reaction (CO_2RR). Lin et al. employed computations (GGA-optB88-vdW level of theory) to study the catalysis of electrochemical CO_2RR on metal surfaces (Au, Ag, Ni, Cu, Pd, Rh and Pt) covered by graphene and revealed that the graphene overlayer reduces the reaction-free energies associated with the intermediate steps.[74] Free energy calculations on these different metal surfaces demonstrated that the presence of the graphene cover significantly reduces the free energy of reaction for $CO_2 + H^+ + e^- \rightarrow$ *COOH (by 4% to 153%) and for *CO $+ H^+ + e^- \rightarrow$ *CHO (by 2% to 19%). Additionally, the graphene overlayer decreases the onset potential for CO_2RR (by 4% to 19%) over different metals considered, with the most significant reduction observed on Ni and Cu surfaces. Analysis of electron density redistribution indicates that there is a partial charge transfer from the π orbitals of graphene to *COOH and *CHO intermediates. This charge transfer occurs from high-energy states to lower-energy states, leading to the reduced repulsion between graphene and the intermediate molecules. The charge transfer from graphene to the adsorbates is influenced by the metal surface, which modulates the Fermi level of the confined system. Notably, stronger charge transfer between graphene and the adsorbate molecules occurs when the underlying metal has a lower Fermi level.

A comparable observation was reported in the case of CO_2RR in graphdiyne (GDY) covered Cu metal using DFT-based studies (RPBE-GGA).[38] The triangular hole in GDY (with 5 Åsides) allows the passage of CO_2 molecule towards the interface with a low energy barrier. In addition, the CO_2 molecule was found to be stabilised under the GDY cover as indicated by a much lower free energy of adsorption (−0.58 eV) as compared to that of the bare Cu(111) surface (−0.04 eV). The adsorbed CO_2 molecule with a higher Fermi level than GDY injects electrons into the GDY and thereby stabilises the GDY-CO_2-Cu system. The PDOS calculation indicates an electron transfer between σ-orbitals of intermediates (*CHO and *COOH) and the π*2p-orbitals of GDY, which allows these adsorbates to be sandwiched between the cover and metal surface, which in turn leads to more negative binding energy of adsorbates (Fig. 14A,B).[38]

In comparison to carbon layers, nitrogen doping in N_x-C layers imparts Lewis base characteristics, enhancing their affinity for acidic CO_2 reactants and significantly increasing the coverage of CO intermediates.[79] DFT calculations by Wang et al. indicate that surface of Cu metal covered by a nitrogen-doped carbon (N–C) layer, facilitates C–C coupling while suppressing the cleavage of the C–O bond in HOCCH*, thus improving ethanol selectivity in CO_2 reduction reactions (CO_2RR). They reported an ethanol Faradaic efficiency (FE) of 52 ±1% and a partial ethanol current density of 156 ±3 mA cm^{-2} using a 34% N–C/Cu catalyst for CO_2RR.[79]

Apart from electronic effects, steric factors also play a critical role in CO_2RR enhancement in confined space.[74,79] For instance, Lin et al. observed that the spacing between graphene and the metal surface depends on the orientations of different adsorbates on the metal surface.[74] The interface height was found to be greater with a CO adsorbate than with a CHO adsorbate because of their differing orientations on the metal. They suggest that variation in binding energy between graphene and the metal surface with changing graphene-metal distance results in an extra energy difference among the metal-CO-graphene and metal-CHO-graphene systems. Here, among various metals, Cu and Ni show a downward trend of the interplanar spacing along

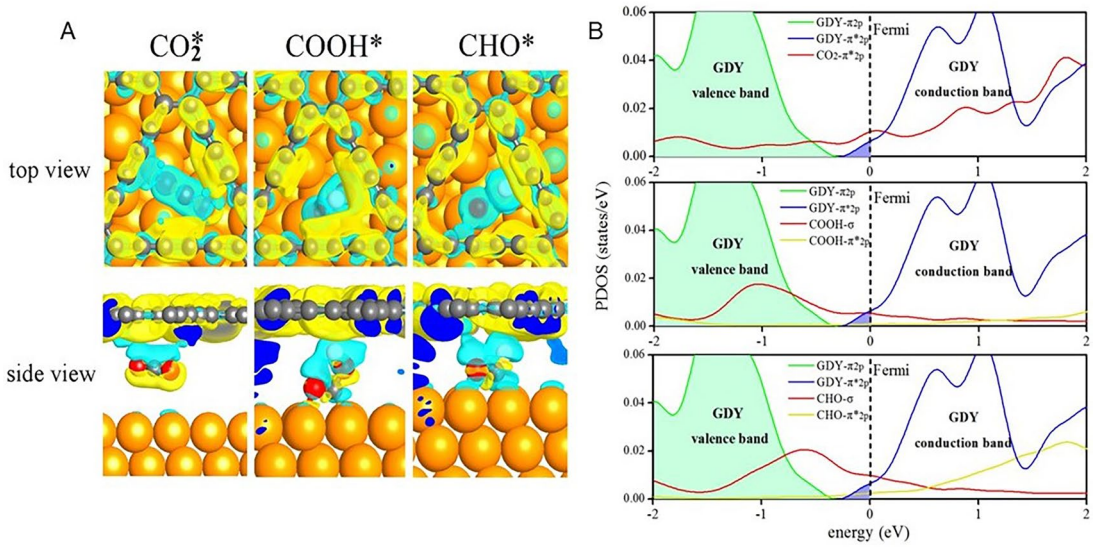

Figure 14: **A** Isosurfaces indicating charge redistribution between the GDY overlayer and the adsorbed intermediates CO_2*, COOH*, and CHO* (isovalues set at ±0.001 e/Å^3; cyan for electron depletion, yellow for accumulation). **B** Projected density of states (PDOS) showing the interaction between GDY electronic bands and the MOs of adsorbed species in Cu-GDY-CO_2, Cu-GDY-COOH, and Cu-GDY-CHO configurations. The Fermi level = 0 V (dotted line), and the populated levels of the valence and conduction bands in GDY are shown in shaded areas. Reprinted from[38] Copyright © 2021, with permission from Elsevier.

the direction of reaction—$CO_2 \rightarrow COOH^* \rightarrow CO^* \rightarrow CHO^*$.[74] In addition, an optimum distance between the metal surface and the overlayer is important to define system stability and product selectivity.[79] For example, DFT calculations by Wang et al. found the N-doped graphene layer at an equilibrium distance of 7.42 Å from the Cu surface. Moreover, the selectivity of ethanol vs. ethylene can be tuned by modulating the distance between N–C overlayer and Cu, ranging from 6.42 Å to 9.42 Å with respect to Cu surface.[79]

4.5 Electrochemical Nitrogen Reduction Reaction

Electrochemical nitrogen reduction reaction (eNRR) has emerged as a promising avenue for generating ammonia under ambient conditions, offering energy efficiency advantages compared to the energy-intensive Haber–Bosch process.[152] Efficiently harnessing the eNRR presents considerable challenges due to the intricate nature of the reaction and its competition with HER. The successful implementation of eNRR hinges on designing novel electrocatalysts that facilitate the activation of inert N_2 molecules while suppressing competing reactions. To address these challenges, researchers have explored various strategies, including surface modification, defect engineering, and electrolyte optimization. Recent advances have shown promising results, with enhanced NH_3 yield and Faradaic efficiencies (FE) achieved through innovative catalyst design and electrochemical cell configuration. Novel electrocatalysts for ammonia synthesis under mild conditions include single-atom catalysts (SACs), MXenes, and metal-organic frameworks (MOFs).[153] However, the effect of 2D confinement on eNRR remains largely unexplored experimentally and theoretically. Studies indicate that 2D confinement influences eNRR kinetics by disrupting the linear scaling relationship between intermediates while also suppressing competing side reactions like HER.[37,78] The following sections explore the eNRR mechanism and the impact of 2D overlayer-induced confinement on eNRR.

4.5.1 Mechanism of eNRR

eNRR is a multistep reaction involving N_2 protonation and electron transfers as illustrated below:

$$N_2(g) + 6H^+(aq) + 6e^- \rightarrow 2NH_3(g) \quad E^0 = 0.056\ V$$

The eNRR pathways are categorized into dissociative and associative, primarily based on the hydrogenation sequences and the mechanism of N≡N bond breaking. In the dissociative mechanism, the N≡N bond breaks during adsorption, leading to the adsorption of dissociated N atoms.

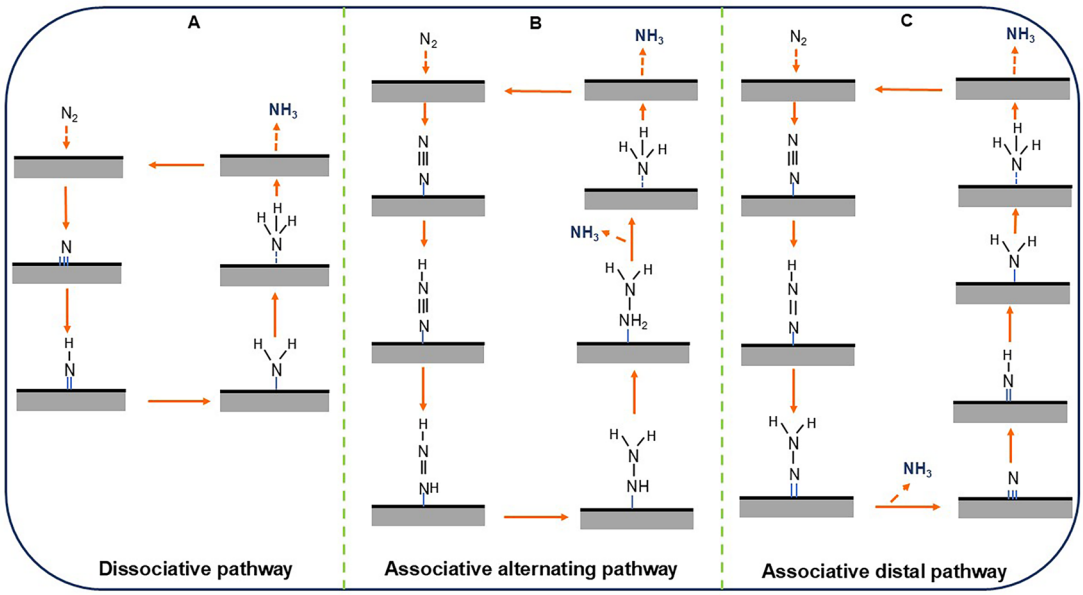

Figure 15: The reaction mechanisms for the eNRR process. **A** dissociative, **B** associative alternating, and **C** associative distal pathways[154].

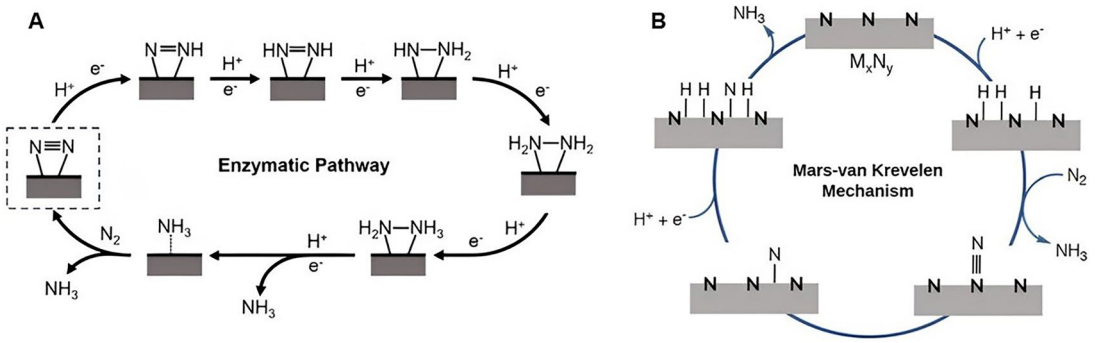

Figure 16: The reaction mechanisms for the electrocatalytic NRR process along **A** the enzymatic pathway. Adapted with permission from[155] Copyright © 2016 American Chemical Society. **B** Mars-van Krevelen (MvK) pathway[156].

Subsequent hydrogenations yield ammonia, which is released in the final step (Fig. 15A).[154] Conversely, the associative mechanism retains the N≡N bond during N_2 adsorption, and the bond cleavage occurs at specific hydrogenation steps. This route can be further generalized into associative, distal (Fig. 15 B,C) and enzymatic pathways (Fig. 16A) based on hydrogenation sequences.

In the distal pathway, terminal nitrogen atoms primarily undergo hydrogenation, with proton addition at surface nitrogen atoms occurring after the release of the remote NH_3 molecule.[157] Along the alternating pathway, hydrogenation shifts among the two N-atoms, with N≡N bond breaking in the final step.[157] The enzymatic pathway involves lateral N_2 adsorption on the catalyst surface initially, followed by similar hydrogenation steps as in the alternating pathway (Fig. 16A). Notably, a new mechanism was proposed, the Mars-van Krevelen (MvK) mechanism where lattice N atoms on transition-metal nitride surfaces are reduced to ammonia, creating N vacancies for continuous eNRR through N_2 adsorption (Fig 16B). The involvement of the surface N atoms of the materials sets this mechanism apart from the conventional ones.[158]

Transition metals (TMs), known for their stability, conductivity, and suitable d orbitals, are promising NRR electrocatalysts. Nørskov

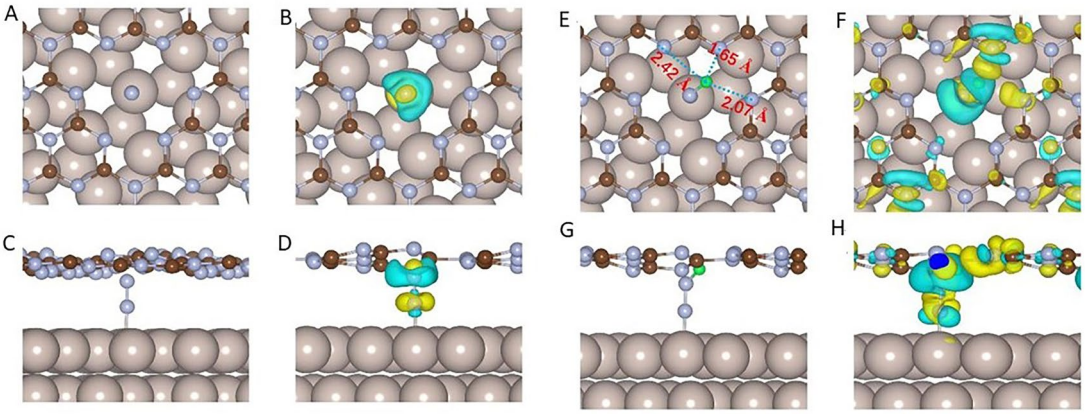

Figure 17: **A**, **C** Illustration of N_2 adsorption on the interface of g-C_3N_4/Ru ; **B**, **D** Charge density variation upon N_2 adsorbed at g-C_3N_4/Ru interface. **E**, **G** Illustration of $*N_2H$ adsorption on Charge density variation of the N_2 adsorbed on g-C_3N_4/Ru interface ; **F**, **H** Charge density variation upon N_2H adsorbed at g-C_3N_4/Ru interface. (oxide red-C, light grey-N, green-H, beige red-Ru. Yellow/cyan indicates charge accumulation/depletion, respectively. Iso-surface values: 0.01 e/AA^3, dashed line—H-bond formed with N) Reprinted from[37] Copyright © 2024 with permission from Elsevier.

and co-workers found that, in the electrochemical synthesis of NH_3 on TMs, the protonation of N_2 to $*N_2H$ or $*NH$ ($*NH_2$) to $*NH_2$ ($*NH_3$) is the typical potential-limiting step.[159–161] They reported that the limiting potential was significantly constrained by the linear scaling between the binding energetics of $*N_2H$ and $*NH$ ($*NH_2$), creating a higher energy barrier slowing down the ammonia synthesis. To mitigate this issue, the introduction of co-adsorbates with stabilising interactions with different intermediate species was suggested, which weakens the linear relationship and improves the reaction kinetics. For example, 2D materials consisting of electronegative elements such as O, N, S, F, etc., are identified as promising candidates for co-adsorbates.[37] HER is a competing side reaction in eNRR, reducing the Faradaic efficiency for ammonia synthesis.[162,163] Hence, assessing the selectivity of nitrogen-fixing catalysts against HER is crucial. Preferably, eNRR catalysts should exhibit a higher overpotential for HER to enhance nitrogen reduction selectivity.

4.5.2 eNRR Under Cover

Wang et al. employed DFT-based (GGA-PBE+D3 level of theory) calculations to study the eNRR activity of Ru and Rh surfaces in the presence of g-C_3N_4 overlayer.[37] This study suggests that incorporation of the g-C_3N_4 overlayer on Ru or Rh surfaces weakens the binding of $*N_2$ while enhancing $*N_2H$ binding, which causes a substantial decrease in the barrier associated with the potential limiting step ($*N_2 + H^+ + e^- \rightarrow *N_2H$) and improvement in NRR catalytic activity compared to pure transition metal surfaces. The van der Waals interactions between Ru and g-C_3N_4 were found to be responsible for bringing $*N_2$ closer to the overlayer, inducing repulsive interactions that destabilise $*N_2$ adsorption in the confined environment. This effect is supported by charge depletion observed between $*N_2$ and g-C_3N_4 (Fig. 17A–D). In contrast, $*N_2H$ adsorption is strengthened due to hydrogen bonding between $*N_2H$ and g-C_3N_4, as confirmed by differential charge density analysis, which reveals charge accumulation at the N–H interaction sites (Fig. 17E–H) Furthermore, the g-C_3N_4 overlayer reduces the limiting potential for NRR while suppressing HER. This study also highlights the potential of leveraging hydrogen bonding and steric confinement to weaken linear scaling relationships, offering a versatile strategy applicable to other catalytic reactions involving protonation steps, such as CO_2 and oxygen reduction reactions.[37] In addition to metal surfaces, clusters of metals such as Fe were found to be catalytically active for eNRR.[164,165] To investigate the impact of confinement on sub-nano metal clusters for eNRR, Wang et al. modeled a confined sub-nanoreactor consisting of Fe_{19} clusters between two 2D layers, g-C_3N_4 and black phosphorus, in a sandwiched form (Fig. 18A).

The Fe_{19} clusters formed stable chemical bonds with both g-C_3N_4 and black phosphorus,

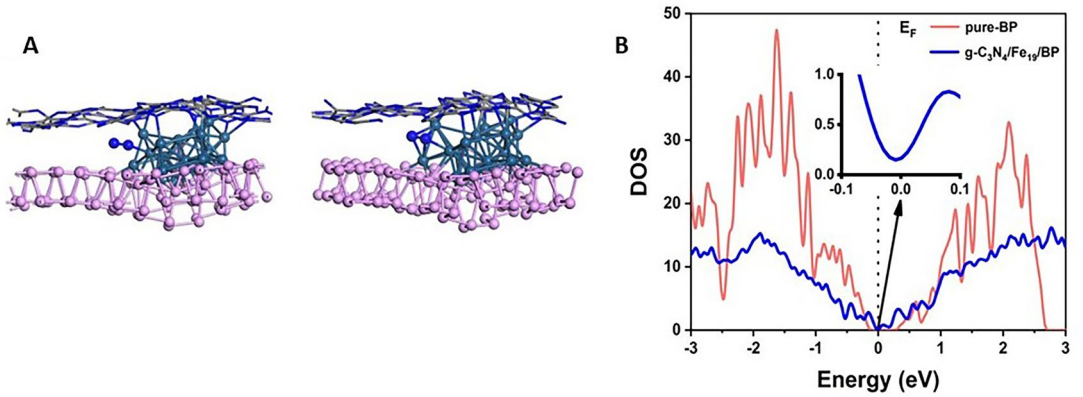

Figure 18: **A** N_2 adsorption configurations on the g-C_3N_4/Fe_{19}/BP system. **B** Computed DOS for the s and p orbitals of 2D BP (pink) and in the C_3N_4/Fe_{19} /BP system (blue). Reprinted from[78] Copyright © 2024 with permission from Elsevier.

preventing mutual aggregation. The computed DOS for the s and p orbitals in the individual BP monolayer and the interface of g-C_3N_4/Fe_{19} / BP show significant broadening of phosphorus atom states upon the formation of the interface. Furthermore, enhanced carrier transport resulted from the generation of novel electronic states at the Fermi level (Fig. 18B). This confined interfacial microenvironment led to a significant reduction in NRR over potential at the Fe active site, decreasing from 0.82 V to 0.49 V. The improved performance is ascribed to the geometric confinement between the two 2D layers and the modified adsorption behaviour of species on the iron cluster in the confined region.[78]

5 Summary and Perspectives

This review explores the role of confined catalysis in small molecule activation, with a particular emphasis on recent computational studies and the insights they provide. The focus is on catalytic systems where confinement is created between 2D layers, applied to reactions such as the hydrogen evolution reaction (HER), oxygen evolution reaction (OER), oxygen reduction reaction (ORR), CO oxidation, CO_2 reduction, and electrocatalytic nitrogen reduction reaction (eNRR). Compared to conventional heterogeneous catalysts, 2D-confined systems offer a tunable chemical environment that stabilises active sites and enhances reaction kinetics. Computational studies suggest the critical role of the effect of structure, electronic structure, defects, charge transfer between the molecule and the catalyst surface, etc., in determining the activity and selectivity of confined catalytic systems. The effect of some of the critical parameters on the catalytic activity under 2D-cover is summarised below:

Charge transfer: 2D-covers alter the adsorption energetics of the reactant molecules by promoting enhanced charge transfer from metal to the adsorbates, which in turn lowers their bond dissociation energy. The adsorption of small molecules like CO on the metal surface is weaker under the influence of 2D-covers, in contrast to the bare metal surface. This optimal interaction prevents catalytic poisoning of the metal surface by the reactant molecules.

Geometric effects: The height of the interface formed between the surface of the metal and the 2D overlayer is crucial for observing the confinement effects. 2D-cover at an optimal distance from the metal surface alters the geometry of the reactants and intermediate molecules.

Defects: While pristine 2D-covers like graphene permit the diffusion of small species such as protons, the presence of defects is crucial to ensure the diffusion of product molecules away from the metal surface. This contributes to the overall stability of the system. In contrast, 2D-covers with an inherent porous structure (eg., graphdiyne) perform more effectively even in the absence of defects, as their pores act as channels for the molecular diffusion. Notably, intermediate species of certain reactions, such as ORR, were found to be stabilised via interactions with undercoordinated atoms at defect sites.

Dopants: The introduction of appropriate dopants into the 2D overlayers is found to act as a channel for molecular diffusion across the layer and facilitate the molecular diffusion across multiple overlayers.

Our literature review reveals that electrocatalytic reactions such as the ORR, CO_2RR, and eNRR have been relatively less explored in the context of 2D-cover-induced confinement. Most of the existing studies focus on catalytic activity arising from confinement between metals/metal oxides and carbon-based materials such as graphene, graphdiyne, h-BN, and g-C_3N_4. In contrast, systems involving defective carbon layers over single-atom catalysts remain largely unexplored and represent a promising direction for future research. Additionally, the fundamental mechanisms of confinement, particularly the role of quantum effects in confined catalysis, remain poorly understood and require more rigorous investigation.

Computational studies, especially those based on DFT, play a crucial role in understanding the mechanisms and factors affecting the performance of the catalytic systems for reactions like HER, OER, and CO_2RR . However, the computational cost associated with higher-level computational approaches and a significant increase in computational cost with increasing system size prevent the efficient exploration of the catalytic reactions.[98,166,167] In this regard, developing novel computational methods to improve the simulation accuracy and facilitate the use of models that mimic realistic experimental conditions is crucial for computational studies of heterogeneous catalysis, especially in confined systems. The development in the field of machine learning potential-based simulations,[168] and *operando* simulations[97] are expected to address these issues to a good extent.

Publisher's Note

Springer Nature remains neutral with regard to jurisdictional claims in published maps and institutional affiliations.

Acknowledgements

AJ thanks the Department of Science and Technology, Government of India, for the INSPIRE fellowship for the Ph.D. program. SK thanks IIT Madras for the New Faculty Seed Grant (NFSG) and the Science and Engineering Research Board (SERB), India, for the funding through the Core Research Grant (CRG/2022/003771). The authors thank Prof. V. Subramanian, IIT Madras, for fruitful discussions.

Declarations

Conflict of Interest

There are no conflicts of interest to declare.

Received: 24 April 2025 Accepted: 18 July 2025
Published online: 20 August 2025

References

1. Peters JC, Mehn MP (2006) Bio-organometallic approaches to nitrogen fixation chemistry. Activation of small molecules. Wiley, Chichester, pp 81–119
2. Milani B, Licini G, Clot E, Albrecht M, Ermert DM, Murray LJ (2016) Themed collection small molecule activation. Dalton Trans 45:14419–14420
3. Kalidindi SB, Jagirdar BR (2013) Nanocatalysis: activation of small molecules and conversion into useful feedstock. In: Nanocatalysis synthesis and applications, pp 679–711
4. Somorjai GA, Li Y (2010) Introduction to surface chemistry and catalysis. Wiley, New York
5. Thomas JM, Thomas WJ (2014) Principles and practice of heterogeneous catalysis. Wiley, New York
6. Fedlheim DL, Foss CA (2001) Metal nanoparticles: synthesis, characterization, and applications. CRC Press, Boca Raton
7. Klabunde KJ, Richards RM (2009) Nanoscale materials in chemistry. Wiley, New York
8. Grunes J, Zhu J, Somorjai GA (2003) Catalysis and nanoscience. Chem Commun 18:2257–2260
9. Yan N (2013) When nanotechnology meets catalysis. Nanotechnol Rev 2(5):485–486
10. Olveira S, Forster SP, Seeger S (2014) Nanocatalysis: academic discipline and industrial realities. J Nanotechnol 1:324089
11. Liu L, Corma A (2018) Metal catalysts for heterogeneous catalysis: from single atoms to nanoclusters and nanoparticles. Chem Rev 118(10):4981–5079
12. Parvulescu VI (2020) Advances in heterogeneous catalysis: concepts of nanocatalysis and single-atom catalysis. ACS Symposium Series. American Chemical Society, pp 1–49
13. Ertl G (2008) Reactions at surfaces: from atoms to complexity (nobel lecture). Angew Chem Int Ed 47(19):3524–3535
14. Campbell CT, Parker SC, Starr DE (2002) The effect of size-dependent nanoparticle energetics on catalyst sintering. Science 298(5594):811–814

15. Obradović MD, Rogan JR, Babić BM, Tripković A, Gautam A, Radmilović VR, Gojković SL (2012) Formic acid oxidation on Pt-Au nanoparticles: relation between the catalyst activity and the poisoning rate. J Power Sources 197:72–79
16. Capon A, Parson R (1973) The oxidation of formic acid at noble metal electrodes: I. review of previous work. J Electroanal Chem Interfacial Electrochem 44(1):1–7
17. Shifa TA, Vomiero A (2019) Confined catalysis: progress and prospects in energy conversion. Adv Energy Mater 9(40):1902307
18. Dong B, Pei Y, Mansour N, Lu X, Yang K, Huang W, Fang N (2019) Deciphering nanoconfinement effects on molecular orientation and reaction intermediate by single molecule imaging. Nat Commun 10(1):4815
19. Grommet AB, Feller M, Klajn R (2020) Chemical reactivity under nanoconfinement. Nat Nanotechnol 15(4):256–271
20. Dong B, Mansour N, Huang T-X, Huang W, Fang N (2021) Single molecule fluorescence imaging of nanoconfinement in porous materials. Chem Soc Rev 50(11):6483–6506
21. Zhang S, Hedtke T, Zhou X, Elimelech M, Kim J-H (2021) Environmental applications of engineered materials with nanoconfinement. ACS ES &T Eng 1(4):706–724
22. Mouarrawis V, Plessius R, Vlugt JI, Reek JN (2018) Confinement effects in catalysis using well-defined materials and cages. Front Chem 6:419863
23. Hoz JM, Balbuena PB (2011) Geometric and electronic confinement effects on catalysis. J Phys Chem C 115(43):21324–21333
24. Leenders SH, Gramage-Doria R, Bruin B, Reek JN (2015) Transition metal catalysis in confined spaces. Chem Soc Rev 44(2):433–448
25. Fei X, Wang P, Zhang D, Wang H, Wu Z (2021) Confined catalysts application in environmental catalysis: current research progress and future prospects. ChemCatChem 13(10):2313–2336
26. Wu S-M, Yang X-Y, Janiak C (2019) Confinement effects in zeolite-confined noble metals. Angew Chem 131(36):12468–12482
27. Romero Ojeda GD, Gomes GJ, Bittencourt PRS, Collins SE, Bosco MV, Peruchena NM, Zalazar MF (2024) Comparative study of adsorbed complexes inside pores and cavities of acid zeolites with different topology Experimental: and theoretical insights into confinement effects. J Phys Chem C 128(17):7137–7148
28. Chai Y, Dai W, Wu G, Guan N, Li L (2021) Confinement in a zeolite and zeolite catalysis. Acc Chem Res 54(13):2894–2904
29. Derouane EG (1998) Zeolites as solid solvents. J Mol Catal A: Chem 134(1–3):29–45
30. Doyle AD, Montoya JH, Vojvodic A (2015) Improving oxygen electrochemistry through nanoscopic confinement. ChemCatChem 7(5):738–742
31. Fu Q, Bao X (2017) Surface chemistry and catalysis confined under two-dimensional materials. Chem Soc Rev 46(7):1842–1874
32. Li H, Xiao J, Fu Q, Bao X (2017) Confined catalysis under two-dimensional materials. Proc Natl Acad Sci 114(23):5930–5934
33. Yao Y, Fu Q, Zhang Y, Weng X, Li H, Chen M, Jin L, Dong A, Mu R, Jiang P et al (2014) Graphene cover-promoted metal-catalyzed reactions. Proc Natl Acad Sci 111(48):17023–17028
34. Guo Y, Chen Y, Duan X (2024) The confined surface C2N/Pt(111) as a highly efficient catalyst for co oxidation. Phys Chem Chem Phys 26(10):8177–8182
35. Lim J, Heo SJ, Jung M, Kim T, Byeon J, Park H, Jang JE, Hong J, Moon J, Pak S et al (2024) Highly sustainable h-BN encapsulated MoS2 hydrogen evolution catalysts. Small 20:2402272
36. Zhao T, Huang X, Cui R, Han W, Zhang G, Tang Z (2023) Design of confined catalysts and applications in environmental catalysis: original perspectives and further prospects. J Clean Prod 390:136125
37. Wang P, Khan AM, Zhao C, Zhu Z, Li C, Wang F, Niu C, Jia Y (2024) Breaking linear scaling relationships in NRR with hydrogen bonding in confined space: a case study of g-C3N4 covered Ru(001) system. Surf Interfaces 47:104219
38. Chen X, Lin Z-Z, Ju M, Guo L-X (2019) Confined electrochemical catalysis under cover: enhanced CO2 reduction at the interface between graphdiyne and Cu surface. Appl Surf Sci 479:685–692
39. Wang S, Feng Y, Yu M, Wan Q, Lin S (2017) Confined catalysis in the $g\text{-}C3N_4$/Pt(111) interface: feasible molecule intercalation, tunable molecule-metal interaction, and enhanced reaction activity of CO oxidation. ACS Appl Mater Interfaces 9(38):33267–33273
40. Tang L, Meng X, Deng D, Bao X (2019) Confinement catalysis with 2D materials for energy conversion. Adv Mater 31(50):1901996
41. Novoselov KS, Mishchenko A, Carvalho A, Castro Neto A (2016) 2D materials and van der Waals heterostructures. Science 353(6298):9439
42. Geim AK, Grigorieva IV (2013) Van der Waals heterostructures. Nature 499(7459):419–425
43. Deng D, Novoselov KS, Fu Q, Zheng N, Tian Z, Bao X (2016) Catalysis with two-dimensional materials and their heterostructures. Nat Nanotechnol 11(3):218–230
44. Ambrosetti A, Silvestrelli PL (2016) Communication: enhanced chemical reactivity of graphene on a Ni(111) substrate. J Chem Phys 144(11):111101
45. Mu R, Fu Q, Jin L, Yu L, Fang G, Tan D, Bao X (2012) Visualizing chemical reactions confined under graphene. Angew Chem (Int Ed Engl) 51(20):4856–4859
46. Zhang Y, Weng X, Li H, Li H, Wei M, Xiao J, Liu Z, Chen M, Fu Q, Bao X (2015) Hexagonal boron nitride cover on Pt(111): a new route to tune molecule-metal

interaction and metal-catalyzed reactions. Nano Lett 15(5):3616–3623
47. Yam KM, Guo N, Jiang Z, Li S, Zhang C (2020) Graphene-based heterogeneous catalysis: role of graphene. Catalysts 10(1):53
48. Sutter P, Sadowski JT, Sutter EA (2010) Chemistry under cover: tuning metal- graphene interaction by reactive intercalation. J Am Chem Soc 132(23):8175–8179
49. Banhart F, Kotakoski J, Krasheninnikov AV (2011) Structural defects in graphene. ACS Nano 5(1):26–41
50. Huang C, Li Y, Wang N, Xue Y, Zuo Z, Liu H, Li Y (2018) Progress in research into 2D graphdiyne-based materials. Chem Rev 118(16):7744–7803
51. Fang Y, Liu Y, Qi L, Xue Y, Li Y (2022) 2D graphdiyne: an emerging carbon material. Chem Soc Rev 51(7):2681–2709
52. Zhao Y, Chai L, Yan X, Huang W, Fan T, Al-Hartomy OA, Al-Ghamdi A, Wageh S, Al-Sehemi AG, Xie Z, Zhang H (2022) Characteristics, properties, synthesis and advanced applications of 2D graphdiyne versus graphene. Mater Chem Front 6(5):528–552
53. Jiao Y, Du A, Hankel M, Zhu Z, Rudolph V, Smith SC (2011) Graphdiyne: a versatile nanomaterial for electronics and hydrogen purification. Chem Commun 47(43):11843–11845
54. Zhang H, He X, Zhao M, Zhang M, Zhao L, Feng X, Luo Y (2012) Tunable hydrogen separation in sp-sp2 hybridized carbon membranes: a first-principles prediction. J Phys Chem C 116(31):16634–16638
55. Chen LX, Jiang M, Lu Z, Gao C, Chen ZW, Singh CV (2021) Two-dimensional graphdiyne-confined platinum catalyst for hydrogen evolution and oxygen reduction reactions. ACS Appl Mater Interfaces 13(40):47541–47548
56. Dai X, Ge D (2018) Numerical investigation on the field emission properties of N-doped graphdiyne-C60 nanostructures. AIP Adv 8(1):015320
57. Naclerio AE, Kidambi PR (2023) A review of scalable hexagonal boron nitride (h-BN) synthesis for present and future applications. Adv Mater 35(6):2207374
58. Yang X, Zhang R, Pu J, He Z, Xiong L (2021) 2D graphene and h-BN layers application in protective coatings. Corros Rev 39(2):93–107
59. Weng Q, Wang X, Wang X, Bando Y, Golberg D (2016) Functionalized hexagonal boron nitride nanomaterials: emerging properties and applications. Chem Soc Rev 45:3989–4012
60. Li LH, Cervenka J, Watanabe K, Taniguchi T, Chen Y (2014) Strong oxidation resistance of atomically thin boron nitride nanosheets. ACS Nano 8(2):1457–1462
61. Ma C, Park J, Liu L, Kim Y-S, Yoon M, Baddorf AP, Gu G, Li A-P (2016) Interplay between intercalated oxygen superstructures and monolayer h-BN on Cu(100). Phys Rev B 94(6):064106
62. Zhang Y, Wei M, Fu Q, Bao X (2015) Oxygen intercalation under hexagonal boron nitride (h-BN) on Pt(111). Sci Bull 60(18):1572–1579
63. Stuart NM, Sohlberg K (2023) A method of calculating surface energies for asymmetric slab models. Phys Chem Chem Phys 25(19):13351–13358
64. Zhou Y, Chen W, Cui P, Zeng J, Lin Z, Kaxiras E, Zhang Z (2016) Enhancing the hydrogen activation reactivity of nonprecious metal substrates via confined catalysis underneath graphene. Nano Lett 16(10):6058–6063
65. Kepenekian M, Traore B, Blancon J-C, Pedesseau L, Tsai H, Nie W, Stoumpos CC, Kanatzidis MG, Even J, Mohite AD, Tretiak S, Katan C (2018) Concept of lattice mismatch and emergence of surface states in two-dimensional hybrid perovskite quantum wells. Nano Lett 18(9):5603–5609
66. Singh-Miller NE, Marzari N (2009) Surface energies, work functions, and surface relaxations of low-index metallic surfaces from first principles. Phys Rev B-Condens Matter Mater Phys 80(23):235407
67. Védrine JC (2017) Heterogeneous catalysis on metal oxides. Catalysts 7(11):341
68. Fishman M, Zhuang HL, Mathew K, Dirschka W, Hennig RG (2013) Accuracy of exchange-correlation functionals and effect of solvation on the surface energy of copper. Phys Rev B: Condens Matter Mater Phys 87(24):245402
69. Lizzit D, Trioni MI, Bignardi L, Lacovig P, Lizzit S, Martinazzo R, Larciprete R (2019) Dual-route hydrogenation of the graphene/Ni interface. ACS Nano 13(2):1828–1838
70. Arulmozhi N, Hanselman S, Tudor V, Chen X, Velden D, Schneider GF, Calle-Vallejo F, Koper MT (2023) Energetics and kinetics of hydrogen electrosorption on a graphene-covered Pt(111) electrode. JACS Au 3(2):526–535
71. Hu K, Ohto T, Nagata Y, Wakisaka M, Aoki Y, Fujita J-I, Ito Y (2021) Catalytic activity of graphene-covered non-noble metals governed by proton penetration in electrochemical hydrogen evolution reaction. Nat Commun 12(1):203
72. Tiwari N, Tiwari AK (2024) Confinement effects of two-dimensional surfaces on water adsorption and dissociation over Pt(111). ChemPhysChem 16:e202400586
73. Tiwari N, Hariharan S, Tiwari AK (2022) Effect of temperature on CO oxidation over Pt(111) in two-dimensional confinement. J Chem Phys 157(14):144701
74. Lin Z-Z, Chen X, Yin C, Yue L, Meng F-X (2020) Electrochemical CO2 reduction in confined space: enhanced activity of metal catalysts by graphene overlayer. Int J Energy Res 44(2):784–794
75. Mao X, Kour G, Yan C, Zhu Z, Du A (2019) Single transition metal atom-doped graphene supported on a nickel substrate: enhanced oxygen reduction reactions

modulated by electron coupling. J Phys Chem C 123(6):3703–3710
76. Xie G, Liu X, Guo B, Tan T, Gong JR (2024) Porous 2D catalyst covers improve photoelectrochemical water-oxidation performance. Adv Mater 36(22):2211008
77. Chen X, Lin Z-Z (2018) Single-layer graphdiyne-covered Pt (111) surface: improved catalysis confined under two-dimensional overlayer. J Nanopart Res 20:1–12
78. Wang B, Diao J, Fu Q, Ma Y (2024) Influence of the confinement effect by a sandwiched subnanoreactor on the electrocatalytic performance for the nitrogen reduction reaction. Appl Surf Sci 656:159715
79. Wang X, Wang Z, Arquer FP, Dinh C-T, Ozden A, Li YC, Nam D-H, Li J, Liu Y-S, Wicks J et al (2020) Efficient electrically powered CO2-to-ethanol via suppression of deoxygenation. Nat Energy 5(6):478–486
80. Wu H, Ren P, Zhao P, Gong Z, Wen X, Cui Y, Fu Q, Bao X (2019) Dynamic nanoscale imaging of enriched CO adlayer on Pt(111) confined under h-BN monolayer in ambient pressure atmospheres. Nano Res 12:85–90
81. Nørskov JK, Rossmeisl J, Logadottir A, Lindqvist L, Kitchin JR, Bligaard T, Jonsson H (2004) Origin of the overpotential for oxygen reduction at a fuel-cell cathode. J Phys Chem B 108(46):17886–17892
82. Kulkarni A, Siahrostami S, Patel A, Nørskov JK (2018) Understanding catalytic activity trends in the oxygen reduction reaction. Chem Rev 118(5):2302–2312
83. Wu C, Shen Y, Wang X, Lv L, Meng X, Jiang X, Gong D, Ai Q, Shuai Y, Zhou Z (2024) Revealing the potential-determining steps of reduction of nitrate to ammonia on transition metal porphyrins catalysts. Surf Interfaces 53:105022
84. Niu S, Li S, Du Y, Han X, Xu P (2020) How to reliably report the overpotential of an electrocatalyst. ACS Energy Lett 5(4):1083–1087
85. Bajdich M, García-Mota M, Vojvodic A, Nørskov JK, Bell AT (2013) Theoretical investigation of the activity of cobalt oxides for the electrochemical oxidation of water. J Am Chem Soc 135(36):13521–13530
86. Rossmeisl J, Logadottir A, Nørskov JK (2005) Electrolysis of water on (oxidized) metal surfaces. Chem Phys 319(1–3):178–184
87. Jonsson H, Mills G, Jacobsen KW (1998) Nudged elastic band method for finding minimum energy paths of transitions. In: Classical and quantum dynamics in condensed phase simulations. World Scientific, pp 385–404
88. Mills G, Jónsson H (1994) Quantum and thermal effects in H2 dissociative adsorption: evaluation of free energy barriers in multidimensional quantum systems. Phys Rev Lett 72(7):1124
89. Henkelman G, Uberuaga BP, Jónsson H (2000) A climbing image nudged elastic band method for finding saddle points and minimum energy paths. J Chem Phys 113(22):9901–9904
90. Sheppard D, Terrell R, Henkelman G (2008) Optimization methods for finding minimum energy paths. J Chem Phys 128(13):134106
91. Henkelman G, Jónsson H (2000) Improved tangent estimate in the nudged elastic band method for finding minimum energy paths and saddle points. J Chem Phys 113(22):9978–9985
92. Zhao G, Rui K, Dou SX, Sun W (2018) Heterostructures for electrochemical hydrogen evolution reaction: a review. Adv Funct Mater 28(43):1803291
93. Strmcnik D, Lopes PP, Genorio B, Stamenkovic VR, Markovic NM (2016) Design principles for hydrogen evolution reaction catalyst materials. Nano Energy 29:29–36
94. Harrington DA, Conway B (1987) ac impedance of faradaic reactions involving electrosorbed intermediates-I. Kinetic theory. Electrochim Acta 32(12):1703–1712
95. Krstajić N, Popović M, Grgur B, Vojnović M, Šepa D (2001) On the kinetics of the hydrogen evolution reaction on nickel in alkaline solution: part I. The mechanism. J Electroanal Chem 512(1–2):16–26
96. Wei J, Zhou M, Long A, Xue Y, Liao H, Wei C, Xu ZJ (2018) Heterostructured electrocatalysts for hydrogen evolution reaction under alkaline conditions. Nano-micro Lett 10:1–15
97. Dattila F, Seemakurthi RR, Zhou Y, López N (2022) Modeling operando electrochemical CO2 reduction. Chem Rev 122(12):11085–11130
98. Miao L, Jia W, Cao X, Jiao L (2024) Computational chemistry for water-splitting electrocatalysis. Chem Soc Rev 53(6):2771–2807
99. Walter C, Menezes PW, Driess M (2021) Perspective on intermetallics towards efficient electrocatalytic water-splitting. Chem Sci 12(25):8603–8631
100. Mahmood N, Yao Y, Zhang J-W, Pan L, Zhang X, Zou J-J (2018) Electrocatalysts for hydrogen evolution in alkaline electrolytes: mechanisms, challenges, and prospective solutions. Adv Sci 5(2):1700464
101. Sheng W, Zhuang Z, Gao M, Zheng J, Chen JG, Yan Y (2015) Correlating hydrogen oxidation and evolution activity on platinum at different pH with measured hydrogen binding energy. Nat Commun 6(1):1–6
102. Fu Y, Rudnev AV, Wiberg GK, Arenz M (2017) Single graphene layer on Pt(111) creates confined electrochemical environment via selective ion transport. Angew Chem Int Ed 56(42):12883–12887
103. Kosmala T, Baby A, Lunardon M, Perilli D, Liu H, Durante C, Di Valentin C, Agnoli S, Granozzi G (2021) Operando visualization of the hydrogen evolution reaction with atomic-scale precision at different metal-graphene interfaces. Nat Catal 4(10):850–859
104. Shih AJ, Arulmozhi N, Koper MT (2021) Electrocatalysis under cover: enhanced hydrogen evolution via defective graphene-covered Pt(111). ACS Catal 11(17):10892–10901

105. Fabbri E, Habereder A, Waltar K, Kötz R, Schmidt TJ (2014) Developments and perspectives of oxide-based catalysts for the oxygen evolution reaction. Catal Sci Technol 4(11):3800–3821
106. Zhang X, Bieberle-Hütter A (2016) Modeling and simulations in photoelectrochemical water oxidation: from single level to multiscale modeling. Chemsuschem 9(11):1223–1242
107. Cheng Y et al (2015) Advances in electrocatalysts for oxygen evolution reaction of water electrolysis-from metal oxides to carbon nanotubes. Prog Nat Sci Mater Int 25(6):545–553
108. Nie Y, Li L, Wei Z (2015) Recent advancements in Pt and Pt-free catalysts for oxygen reduction reaction. Chem Soc Rev 44(8):2168–2201
109. Xiao L, Zhuang L, Liu Y, Lu J (2009) Activating Pd by morphology tailoring for oxygen reduction. J Am Chem Soc 131(2):602–608
110. Suo Y, Zhuang L, Lu J (2007) First-principles considerations in the design of Pd-alloy catalysts for oxygen reduction. Angew Chem Int Ed 46(16):2862–2864
111. Liu Y, Le Formal F, Boudoire F, Guijarro N (2019) Hematite photoanodes for solar water splitting: a detailed spectroelectrochemical analysis on the pH-dependent performance. ACS Appl Energy Mater 2(9):6825–6833
112. Wang Y, Zhang Y, Liu Z, Xie C, Feng S, Liu D, Shao M, Wang S (2017) Layered double hydroxide nanosheets with multiple vacancies obtained by dry exfoliation as highly efficient oxygen evolution electrocatalysts. Angew Chem Int Ed 56(21):5867–5871
113. Dou Y, Liao T, Ma Z, Tian D, Liu Q, Xiao F, Sun Z, Kim JH, Dou SX (2016) Graphene-like holey Co3O4 nanosheets as a highly efficient catalyst for oxygen evolution reaction. Nano Energy 30:267–275
114. Curutchet A, Colinet P, Michel C, Steinmann SN, Le Bahers T (2020) Two-sites are better than one: revisiting the OER mechanism on CoOOH by DFT with electrode polarization. Phys Chem Chem Phys 22(13):7031–7038
115. Yan Z, Liu H, Hao Z, Yu M, Chen X, Chen J (2020) Electrodeposition of (hydro) oxides for an oxygen evolution electrode. Chem Sci 11(39):10614–10625
116. Liang Q, Brocks G, Bieberle-Hütter A (2021) Oxygen evolution reaction (OER) mechanism under alkaline and acidic conditions. J Phys Energy 3(2):026001
117. Li H, Kelly S, Guevarra D, Wang Z, Wang Y, Haber JA, Anand M, Gunasooriya GKK, Abraham CS, Vijay S et al (2021) Analysis of the limitations in the oxygen reduction activity of transition metal oxide surfaces. Nat Catal 4(6):463–468
118. Zhao Y, Adiyeri Saseendran DP, Huang C, Triana CA, Marks WR, Chen H, Zhao H, Patzke GR (2023) Oxygen evolution/reduction reaction catalysts: from in situ monitoring and reaction mechanisms to rational design. Chem Rev 123(9):6257–6358
119. Ibrahim KB, Tsai M-C, Chala SA, Berihun MK, Kahsay AW, Berhe TA, Su W-N, Hwang B-J (2019) A review of transition metal-based bifunctional oxygen electrocatalysts. J Chin Chem Soc 66(8):829–865
120. Wang H, Zhang KH, Hofmann JP, Oropeza FE et al (2021) The electronic structure of transition metal oxides for oxygen evolution reaction. J Mater Chem A 9(35):19465–19488
121. Greeley J, Stephens I, Bondarenko A, Johansson TP, Hansen HA, Jaramillo T, Rossmeisl J, Chorkendorff I, Nørskov JK (2009) Alloys of platinum and early transition metals as oxygen reduction electrocatalysts. Nat Chem 1(7):552–556
122. Zhu L, Wu J, Zhang Q, Li X, Li Y, Cao X (2018) Chemical-free fabrication of n, p dual-doped honeycomb-like carbon as an efficient electrocatalyst for oxygen reduction. J Colloid Interface Sci 510:32–38
123. Xia BY, Yan Y, Li N, Wu HB, Lou XWD, Wang X (2016) A metal-organic framework-derived bifunctional oxygen electrocatalyst. Nat Energy 1(1):1–8
124. Hong WT, Risch M, Stoerzinger KA, Grimaud A, Suntivich J, Shao-Horn Y (2015) Toward the rational design of non-precious transition metal oxides for oxygen electrocatalysis. Energy Environ Sci 8(5):1404–1427
125. Ling C, Shi L, Ouyang Y, Zeng XC, Wang J (2017) Nanosheet supported single-metal atom bifunctional catalyst for overall water splitting. Nano Lett 17(8):5133–5139
126. Ferrighi L, Datteo M, Fazio G, Di Valentin C (2016) Catalysis under cover: enhanced reactivity at the interface between (doped) graphene and anatase TiO2. J Am Chem Soc 138(23):7365–7376
127. Jiang Q, Ao Z, Li S, Wen Z (2014) Density functional theory calculations on the CO catalytic oxidation on al-embedded graphene. RSC Adv 4(39):20290–20296
128. Poerwoprajitno AR, Gloag L, Watt J, Cheong S, Tan X, Lei H, Tahini HA, Henson A, Subhash B, Bedford NM et al (2022) A single-Pt-atom-on-Ru-nanoparticle electrocatalyst for CO-resilient methanol oxidation. Nat Catal 5(3):231–237
129. Qiao B, Wang A, Yang X, Allard LF, Jiang Z, Cui Y, Liu J, Li J, Zhang T (2011) Single-atom catalysis of CO oxidation using Pt_1/FeO_x. Nat Chem 3(8):634–641
130. Zhao S, Wang T, Ji Z, Song Y, Li Y, Liu J, Hu W (2023) Spatial decoupling of dehydrogenation and CO oxidation by Ni-Co-Ti hierarchical trimetallic catalyst for electrocatalytic oxidation of methanol. Appl Catal B 320:122024
131. Zhang H, Fang S, Hu YH (2022) Recent advances in single-atom catalysts for CO oxidation. Catal Rev 64(3):491–532
132. Liu H, Jia R, Qin C, Yang Q, Tang Z, Li M, Ma Z (2023) Anti-CO poisoning FePtRh nanoflowers with Rh-rich core and Fe-rich shell boost methanol oxidation electrocatalysis. Adv Funct Mater 33(7):2210626

133. Granas E, Andersen M, Arman MA, Gerber T, Hammer B, Schnadt J, Andersen JN, Michely T, Knudsen J (2013) CO intercalation of graphene on Ir(111) in the millibar regime. J Phys Chem C 117(32):16438–16447
134. Wei F, Wan Q, Lin S, Guo H (2020) Origin of confined catalysis in nanoscale reactors between two-dimensional covers and metal substrates: mechanical or electronic? J Phys Chem C 124(21):11564–11573
135. Domagala ME, Campbell CT (1991) The mechanism of CO oxidation over Cu(110): effect of CO gas energy. Catal Lett 9:65–70
136. Baxter R, Hu P (2002) Insight into why the Langmuir–Hinshelwood mechanism is generally preferred. J Chem Phys 116(11):4379–4381
137. Kuipers E, Vardi A, Danon A, Amirav A (1991) Surface-molecule proton transfer: a demonstration of the Eley–Rideal mechanism. Phys Rev Lett 66(1):116
138. Rettner C (1992) Dynamics of the direct reaction of hydrogen atoms adsorbed on Cu(111) with hydrogen atoms incident from the gas phase. Phys Rev Lett 69(2):383
139. Eads CN, Boscoboinik JA, Head AR, Hunt A, Waluyo I, Stacchiola DJ, Tenney SA (2021) Enhanced catalysis under 2D silica: a CO oxidation study. Angew Chem 133(19):10983–10989
140. Hong J, Zhang W, Ren J, Xu R (2013) Photocatalytic reduction of CO_2: a brief review on product analysis and systematic methods. Anal Methods 5(5):1086–1097
141. Hori Y, Wakebe H, Tsukamoto T, Koga O (1994) Electrocatalytic process of CO selectivity in electrochemical reduction of CO2 at metal electrodes in aqueous media. Electrochim Acta 39(11–12):1833–1839
142. Kuhl KP, Hatsukade T, Cave ER, Abram DN, Kibsgaard J, Jaramillo TF (2014) Electrocatalytic conversion of carbon dioxide to methane and methanol on transition metal surfaces. J Am Chem Soc 136(40):14107–14113
143. Tian H, Yang H, Liu X, Jia Y, Xu Q (2025) Confinement effect on the electrochemical CO2 reduction reaction. Green Chem 27:1238–1253
144. Hori Y (2008) In: Vayenas CG, White RE, Gamboa-Aldeco ME (eds) Electrochemical CO2 reduction on metal electrodes. Springer, New York, pp 89–189
145. Appel AM, Bercaw JE, Bocarsly AB, Dobbek H, DuBois DL, Dupuis M, Ferry JG, Fujita E, Hille R, Kenis PJ et al (2013) Frontiers, opportunities, and challenges in biochemical and chemical catalysis of CO2 fixation. Chem Rev 113(8):6621–6658
146. Kang P, Cheng C, Chen Z, Schauer CK, Meyer TJ, Brookhart M (2012) Selective electrocatalytic reduction of CO2 to formate by water-stable iridium dihydride pincer complexes. J Am Chem Soc 134(12):5500–5503
147. Durand WJ, Peterson AA, Studt F, Abild-Pedersen F, Nørskov JK (2011) Structure effects on the energetics of the electrochemical reduction of CO2 by copper surfaces. Surf Sci 605(15–16):1354–1359
148. Todorova TK, Schreiber MW, Fontecave M (2019) Mechanistic understanding of CO2 reduction reaction (CO2RR) toward multicarbon products by heterogeneous copper-based catalysts. ACS Catal 10(3):1754–1768
149. Khalil M, Kadja GTM, Nugroho FAA, Sutanto LG, Jiwanti PK, Abdi FF, Hussin F, Aroua MK (2024) Suppressing the competing hydrogen evolution reaction in CO2 electroreduction: a review. Renew Sustain Energy Rev 206:114869
150. Peterson AA, Nørskov JK (2012) Activity descriptors for CO2 electroreduction to methane on transition-metal catalysts. J Phys Chem Lett 3(2):251–258
151. Shi C, Hansen HA, Lausche AC, Nørskov JK (2014) Trends in electrochemical CO2 reduction activity for open and close-packed metal surfaces. Phys Chem Chem Phys 16(10):4720–4727
152. Marnellos G, Stoukides M (1998) Ammonia synthesis at atmospheric pressure. Science 282(5386):98–100
153. Chebrolu VT, Jang D, Rani GM, Lim C, Yong K, Kim WB (2023) Overview of emerging catalytic materials for electrochemical green ammonia synthesis and process. Carbon Energy 5(12):361
154. Shipman MA, Symes MD (2017) Recent progress towards the electrosynthesis of ammonia from sustainable resources. Catal Today 286:57–68
155. Li X-F, Li Q-K, Cheng J, Liu L, Yan Q, Wu Y, Zhang X-H, Wang Z-Y, Qiu Q, Luo Y (2016) Conversion of dinitrogen to ammonia by FeN3-embedded graphene. J Am Chem Soc 138(28):8706–8709
156. Cui L, Sun Z, Wang Y, Jian X, Li H, Zhang X, Gao X, Li R, Liu J (2024) *H migration-assisted MvK mechanism for efficient electrochemical NH3 synthesis over TM-TiNO. Phys Chem Chem Phys 26(21):15705–15716
157. Shi L, Yin Y, Wang S, Sun H (2020) Rational catalyst design for N2 reduction under ambient conditions: strategies toward enhanced conversion efficiency. ACS Catal 10(12):6870–6899
158. Mars P, Van Krevelen DW (1954) Oxidations carried out by means of vanadium oxide catalysts. Chem Eng Sci 3:41–59
159. Howalt JG, Bligaard T, Rossmeisl J, Vegge T (2013) DFT based study of transition metal nano-clusters for electrochemical NH3 production. Phys Chem Chem Phys 15(20):7785–7795
160. Skulason E, Bligaard T, Gudmundsdóttir S, Studt F, Rossmeisl J, Abild-Pedersen F, Vegge T, Jónsson H, Nørskov JK (2012) A theoretical evaluation of possible transition metal electro-catalysts for N2 reduction. Phys Chem Chem Phys 14(3):1235–1245
161. Montoya JH, Tsai C, Vojvodic A, Nørskov JK (2015) The challenge of electrochemical ammonia synthesis:

a new perspective on the role of nitrogen scaling relations. Chemsuschem 8(13):2180–2186

162. Choi J, Suryanto BH, Wang D, Du H-L, Hodgetts RY, Ferrero Vallana FM, MacFarlane DR, Simonov AN (2020) Identification and elimination of false positives in electrochemical nitrogen reduction studies. Nat Commun 11(1):5546
163. Choi C, Gu GH, Noh J, Park HS, Jung Y (2021) Understanding potential-dependent competition between electrocatalytic dinitrogen and proton reduction reactions. Nat Commun 12(1):4353
164. Wang X, Zhao Y, Wang L, Peng W, Feng J, Li D, Su B-J, Juang J-Y, Ma Y, Chen Y et al (2022) Regulating the electronic configuration of supported iron nanoparticles for electrochemical catalytic nitrogen fixation. Adv Funct Mater 32(21):2111733
165. Jin W, Feng A, He T, Li D, Qu B, Zhou R (2024) Small-sized Fen clusters supported on the anatase TiO2 (101) surface as a promising high-performance catalyst for the N2 reduction reaction. J Phys Chem C 128(24):9993–10006
166. Zeng CM, Panetier JA (2025) Computational modeling of electrocatalysts for CO2 reduction: probing the role of primary, secondary, and outer coordination spheres. Acc Chem Res 58:342–353
167. Xu A, Govindarajan N, Kastlunger G, Vijay S, Chan K (2022) Theories for electrolyte effects in CO2 electroreduction. Acc Chem Res 55(4):495–503
168. Wang Y, Shao H, Zhang C, Liu F, Zhao J, Zhu S, Leung MKH, Hu J (2023) Molecular dynamics for electrocatalysis: mechanism explanation and performance prediction. Energy Rev 2(3):100028

Athira Jayasankar received her Master's degree in Chemistry from Maharaja's College, Ernakulam, Kerala, in 2023. She is currently pursuing her Ph.D. under the supervision of Dr. Sooraj Kunnikuruvan at the Indian Institute of Technology Madras. Her research interest focuses on computational studies on the development of catalytic systems for 'confined catalysis' with applications to energy storage and small molecule activation.

Sooraj Kunnikuruvan has been an Assistant Professor in the Department of Chemistry at the Indian Institute of Technology (IIT) Madras since May 2022. He received his Ph.D. in Chemistry from IIT Kanpur in 2018, followed by two years of post-doctoral research at Bar-Ilan University, Israel. In October 2020, he began his independent research career as an INSPIRE Faculty Fellow at IISER Thiruvananthapuram. Dr. Kunnikuruvan's research focuses on the computational investigation of chemical reactions occurring at interfaces, with particular emphasis on their applications in catalysis and energy storage technologies.